ELEMENTA
Science of the Anthropocene

Mellat, M, et al. 2024. Isotopic signatures of snow, sea ice, and surface seawater in the central Arctic Ocean during the MOSAiC expedition. *Elem Sci Anth*, 12: 1. DOI: https://doi.org/10.1525/elementa.2023.00078

RESEARCH ARTICLE

Isotopic signatures of snow, sea ice, and surface seawater in the central Arctic Ocean during the MOSAiC expedition

Moein Mellat[1,2,*], Camilla F. Brunello[3], Martin Werner[3], Dorothea Bauch[4,5], Ellen Damm[1], Michael Angelopoulos[1], Daiki Nomura[6], Jeffrey M. Welker[7,8,9], Martin Schneebeli[10], Mats A. Granskog[11], Maria Hoerhold[3], Amy R. Macfarlane[10], Stefanie Arndt[3], and Hanno Meyer[1]

The Arctic Ocean is an exceptional environment where hydrosphere, cryosphere, and atmosphere are closely interconnected. Changes in sea-ice extent and thickness affect ocean currents, as well as moisture and heat exchange with the atmosphere. Energy and water fluxes impact the formation and melting of sea ice and snow cover. Here, we present a comprehensive statistical analysis of the stable water isotopes of various hydrological components in the central Arctic obtained during the Multidisciplinary drifting Observatory for the Study of Arctic Climate (MOSAiC) expedition in 2019–2020, including the understudied Arctic winter. Our dataset comprises >2200 water, snow, and ice samples. Snow had the most depleted and variable isotopic composition, with $\delta^{18}O$ (–16.3‰) increasing consistently from surface (–22.5‰) to bottom (–9.7‰) of the snowpack, suggesting that snow metamorphism and wind-induced transport may overprint the original precipitation isotope values. In the Arctic Ocean, isotopes also help to distinguish between different sea-ice types, and whether there is a meteoric contribution. The isotopic composition and salinity of surface seawater indicated relative contributions from different freshwater sources: lower $\delta^{18}O$ (approximately –3.0‰) and salinities were observed near the eastern Siberian shelves and towards the center of the Transpolar Drift due to river discharge. Higher $\delta^{18}O$ (approximately –1.5‰) and salinities were associated with an Atlantic source when the RV *Polarstern* crossed the Gakkel Ridge into the Nansen Basin. These changes were driven mainly by the shifts within the Transpolar Drift that carried the *Polarstern* across the Arctic Ocean. Our isotopic analysis highlights the importance of investigating isotope fractionation effects, for example, during sea-ice formation and melting. A systematic full-year sampling for water isotopes from different components strengthens our understanding of the Arctic water cycle and provides crucial insights into the interaction between atmosphere, sea ice, and ocean and their spatio-temporal variations during MOSAiC.

Keywords: Arctic, MOSAiC expedition, Snow, Sea ice, Seawater, Stable water isotopes

1. Introduction

The Arctic is experiencing warming that is four times the global rate, with cascading consequences affecting major biogeochemical cycles (Vihma et al., 2016; Arctic Monitoring and Assessment Programme, 2017; Pörtner et al., 2022). For instance, the Arctic water cycle, encompassing precipitation, evaporation, and water transport through rivers, oceans, and sea ice, is undergoing notable changes which may, in turn, impact global climate and ocean circulation (Polyakov et al., 2018). In the past 20 years, the Arctic's surface air

[1] Alfred Wegener Institute Helmholtz Centre for Polar and Marine Research, Potsdam, Germany
[2] Institute for Environment Science and Geography, University of Potsdam, Potsdam, Germany
[3] Alfred Wegener Institute Helmholtz Centre for Polar and Marine Research, Bremerhaven, Germany
[4] Leibniz-Laboratory, University of Kiel CAU, Kiel, Germany
[5] GEOMAR Helmholtz Centre for Ocean Research, Kiel, Germany
[6] Field Science Center for Northern Biosphere, Hokkaido University, Hakodate, Hokkaido, Japan
[7] Ecology and Genetics Research Unit, University of Oulu, Oulu, Finland
[8] University of the Arctic (UArctic), Rovaniemi, Finland
[9] Department of Biological Sciences, University of Alaska Anchorage, Anchorage, AK, USA
[10] WSL Institute for Snow and Avalanche Research SLF, Davos, Switzerland
[11] Norwegian Polar Institute, Fram Centre, Tromsø, Norway
* Corresponding author:
Email: moein.mellat@awi.de

temperature has risen by approximately 1.7°C compared to the long-term average (Overland et al., 2019), having distinct effects on the cryosphere, especially in major reductions in sea ice (Parkinson and DiGirolamo, 2021), and variations in precipitation patterns (Rieke et al., 2023). In particular, the loss of sea ice is critical, as sea ice regulates the energy exchange between the ocean and the atmosphere (Serreze et al., 2006; Stroeve et al., 2012; Sun et al., 2022). A reduced sea-ice cover leads to increased evaporation which, in turn, fuels moisture transport into and out of the Arctic (Klein et al., 2015; Mellat et al., 2021). These sea-ice changes also amplify atmospheric blocking patterns over Europe, resulting in extreme snowfall across Scandinavia and Western Europe (Bailey et al., 2021). The consequences of cryospheric changes in the Arctic water cycle are far-reaching and have global implications, given that the melting of sea ice has the potential to modify ocean currents and weather patterns, ultimately influencing climate conditions in middle and lower latitudes (Puntsag et al., 2016; Screen et al., 2018). Essential to improving our understanding of the causes and consequences of the Arctic changes is to collect direct year-round observations and to use these data to benchmark climate models that can then be used to forecast future Arctic scenarios, such as one that is ice-free in the summer (Lindsay and Schweiger, 2015).

The lack of observations in the central Arctic Ocean limits our understanding of the Arctic water cycle and hampers the projection of its future changes. The Multidisciplinary drifting Observatory for the Study of Arctic Climate (MOSAiC) expedition aimed to improve models of the Arctic climate system and fill knowledge gaps by gathering extensive field data (Nicolaus et al., 2022; Rabe et al., 2022; Shupe et al., 2022). This year-long expedition started in September 2019 with the German research icebreaker *Polarstern* (Knust, 2017) frozen into the sea ice north of the Laptev Sea (Krumpen et al., 2020). The ship and surrounding observatory then drifted with the ice within the Transpolar Drift (TPD) for the following 12 months. This expedition provided the opportunity to collect an extensive number of discrete water samples from multiple hydrological components to learn about the exchange processes between the ocean, cryosphere, ecosystems, and atmosphere around the *Polarstern* during an entire hydrological year, including the transition from a frozen ocean state to open seawater conditions (Nicolaus et al., 2022).

1.1. Stable water isotopes and fractionation processes affecting them

Stable water isotopologues, H_2O^{16}, H_2O^{18}, and $HD^{16}O$, hereafter referred to as water isotopes, are excellent proxies for past climate changes and the modern water cycle due to their temperature-dependent fractionation, which occurs during water phase transitions (Dansgaard, 1964; Rozanski et al., 1992; Gat, 1996; Galewsky et al., 2016; Bowen et al., 2019). Isotopic fractionation is a term describing the preferential partitioning of isotopes during physical and chemical processes (Dansgaard, 1964). Equilibrium fractionation occurs when a system achieves a state of isotopic equilibrium, wherein isotopic exchanges occur with the surrounding environment. This equilibrium fractionation process not only is influenced by the specific conditions of the system but also exhibits a pronounced temperature dependence. Non-equilibrium fractionation, on the other hand, occurs when the isotopic composition of water molecules changes due to kinetic processes (i.e., one-way reactions), such as evaporation, condensation, or other phase transitions. These processes can cause a separation between the isotopes of hydrogen and oxygen, leading to a deviation from the expected equilibrium relationship. Essentially, this deviation provides information about the non-equilibrium conditions that exist during the evaporation process, where the slower diffusion of heavy isotopes results in the enrichment of deuterium in the evaporated water vapor. These non-equilibrium conditions are influenced by factors such as humidity gradients and wind advection, which prevent isotopic equilibrium from being reached between the liquid and gas phases (Pfahl and Sodemann, 2014).

The measurement of $\delta^{18}O$ and $\delta^{2}H$ involves determining the ratio of heavy to light isotopes relative from a standard, typically Vienna Standard Mean Ocean Water (V-SMOW standard). The results are expressed in delta (δ) notation, which quantifies the proportion of the isotope ratio of the sample and the standard in per mil (‰). The Global Meteoric Water Line (GMWL) is a linear relationship between the isotopic composition of precipitation and temperature on a global scale (Gat, 1996). To quantify the extent of deviation from the GMWL, a second-order parameter called deuterium excess ($d\text{-}excess = \delta^2H - 8 * \delta^{18}O$; Craig, 1961) is used.

1.2. Water isotopes in the Arctic water cycle

Isotopes are highly sensitive tracers of moisture exchanges between the atmosphere, ocean, and cryosphere, with each component exhibiting a unique isotopic composition (Jouzel, 2003; Klein and Welker, 2016). The isotopic composition of water is affected by origin and transport of the moisture which results in altitudinal and latitudinal gradients (Johnsen et al., 1989; Dutton et al., 2005; Welker, 2012; Terzer-Wassmuth et al., 2021) that reflect the origin and transport of moisture from various sources, including oceanic and continental regions (Hoffmann et al., 2000; Steen-Larsen et al., 2014; Akers et al., 2020; Mellat et al., 2021). The isotopic composition of water is affected by evaporation, condensation due to rainout processes during transport from oceans to continents (Winnick et al., 2014), and by the formation and melting of ice (Eicken, 1998; Granskog et al., 2017; Tian et al., 2018). Therefore, water isotopes provide an integrated tracer of moisture exchange between phases, conditions, and across different components of the water cycle (Aron et al., 2023).

1.2.1. Precipitation

The isotopic values of winter precipitation are typically depleted in $\delta^{18}O$ and $\delta^{2}H$ values in contrast to summer precipitation (Welker, 2000; Bailey et al., 2019), primarily as a result of temperature-dependent isotope fractionation (Dansgaard, 1964). During winter, the air is colder,

and the amount of moisture in the atmosphere is lower. Additionally, winter storms tend to originate from more northerly latitudes (Puntsag et al., 2016; Bailey et al., 2019; Bailey et al., 2021; Brunello et al., 2023), where the moisture sources have already undergone considerable fractionation due to lower temperatures. Hence, the effect of seasonality on the isotopic composition of precipitation should be most pronounced at the surface, where snow is added. Furthermore, frost flowers, icy crystals resulting from water vapor recrystallization, form on nascent ice (Style and Worster, 2009). Composed of delicate needle-like crystals, these structures extend several centimeters from the ice surface. Notably, the isotopic composition of frost flowers offers a compelling measure due to their emergence process, wherein they provide a means to track the impact of vapor isotopes. This tracking ability is because frost flowers form when warm air encounters colder ice. In Arctic regions, they emerge on newly frozen leads during warmer intervals, allowing freezing from brine channels (Barber et al., 2014). Consequently, these frost flowers possess higher sea salt concentrations than surrounding ice, snow, and air (Douglas et al., 2012).

1.2.2. Seawater

The isotopic composition of Arctic Ocean water is influenced by sea-ice formation and sea-ice and snow melting, precipitation, and meteoric freshwater input from rivers and glaciers (Laukert et al., 2017; Paffrath et al., 2021; Solomon et al., 2021; Wefing et al., 2022). The Arctic Ocean is characterized by a more depleted water in heavy isotopes than compared to other ocean regions (Östlund and Hut, 1984) due to its high latitude and the westerly circulation system over Eurasia. Melting of sea ice and snow during summer causes the $\delta^{18}O$ and $\delta^{2}H$ values of the surrounding water to decrease due to the addition of freshwater depleted in $\delta^{18}O$ (Lehmann and Siegenthaler, 1991; Csank et al., 2019). Furthermore, the Arctic Ocean receives freshwater from major rivers like the Ob, Yenisei, and Lena. These rivers have lower salinity and lower $\delta^{18}O$ and $\delta^{2}H$ values, signifying a substantial riverine influx and thus underscoring the significant influence of freshwater on the seawater geochemistry of the Arctic Ocean, particularly at the surface (Cooper et al., 2005; Bauch et al., 2011a; Dubinina et al., 2017).

1.2.3. Sea ice

The Arctic hydrological system experiences significant influence from sea ice, a critical and dynamic element within the water cycle, which also influences processes of ocean-atmosphere exchange (Eicken, 1998; Deser and Teng, 2008; Toyota et al., 2013; Chemke et al., 2021; Smith et al., 2022). Within this context, stable water isotopes offer valuable insights into freezing mechanisms, where the degree of kinetic isotopic fractionation is directly linked to the isotopic composition of surface water and the freezing rate, as demonstrated by Jouzel et al. (1999). To illustrate, regions in closer proximity to continental freshwater sources, exemplified by the Siberian rivers in the Kara and Laptev Sea areas, foster the formation of relatively isotopically light, ^{18}O-depleted sea ice. Consequently, this phenomenon contributes to the formation of sea ice characterized by lower $\delta^{18}O$ values. This specific type of sea ice has the potential to be transported across the central Arctic through mechanisms like the TPD, as evidenced by the findings of Granskog et al. (2017). In this manner, the interplay of water isotopes and freezing dynamics emerges as a crucial factor in the intricate processes of the Arctic hydrological system.

Further, water balance calculations suggest that besides sea ice, meltwater from the snow cover and direct precipitation can contribute significantly to the evolution of melt ponds and leads during the sea-ice melt season (Webster et al., 2015; Nomura et al., 2023). While the contribution of melt ponds and leads as local sources of water vapor remains a topic of debate (Tian et al., 2018), clarifying their roles is important. Leads are narrow and often linear cracks in the sea ice, generated by wind and ocean currents (Wang et al., 2016). During a lead formation, the seawater underneath the ice cover is suddenly exposed to the surface. In winter, leads typically refreeze in a few hours depending on the air temperature (Perovich and Richter-Menge, 1994). Melt ponds, on the other hand, are reservoirs of water formed from surface melt of snow and sea ice (Webster et al., 2022). These ponds form on the sea ice during the spring and summer seasons, corresponding to rising ambient air temperatures (Hanisco et al., 2007). Therefore, quantifying the isotopic composition of sea ice, its snow cover, and the processes affecting its formation and melting is crucial for assessing the complex interactions between individual components of the Arctic hydrological system.

This article aims to explore the isotopic ($\delta^{18}O$, $\delta^{2}H$, *d-excess*) composition of various components in the Arctic Ocean system during the MOSAiC campaign, with a focus on snow, sea ice, and seawater. To better understand water sources and mixing processes for the individual components of the Arctic water cycle, we use the overall statistics of the isotope dataset as well as the spatial-temporal changes of each hydrological component during the MOSAiC expedition. Finally, we characterize the key factors influencing the isotopic composition and the interaction between different hydrological components throughout the year. By doing so, we aim to provide a background dataset of the isotopic signatures of different water components in the central Arctic Ocean and their spatio-temporal changes for different types of sea ice, snow, and seawater. Our goal is to learn which key mechanisms control the fractionation of isotopes during sea-ice formation and melting, what are the contributions of different water sources to the Arctic Ocean's isotopic composition, and how changes in these sources affect the Arctic water cycle over time.

2. Methods and materials

2.1. MOSAiC expedition

The MOSAiC expedition took place from October 2019 to September 2020. During this time, the *Polarstern* drifted across the central Arctic Ocean, frozen in the sea ice (Nicolaus et al., 2022; Rabe et al., 2022; Shupe et al., 2022). The MOSAiC expedition was divided into 5 phases, so-called

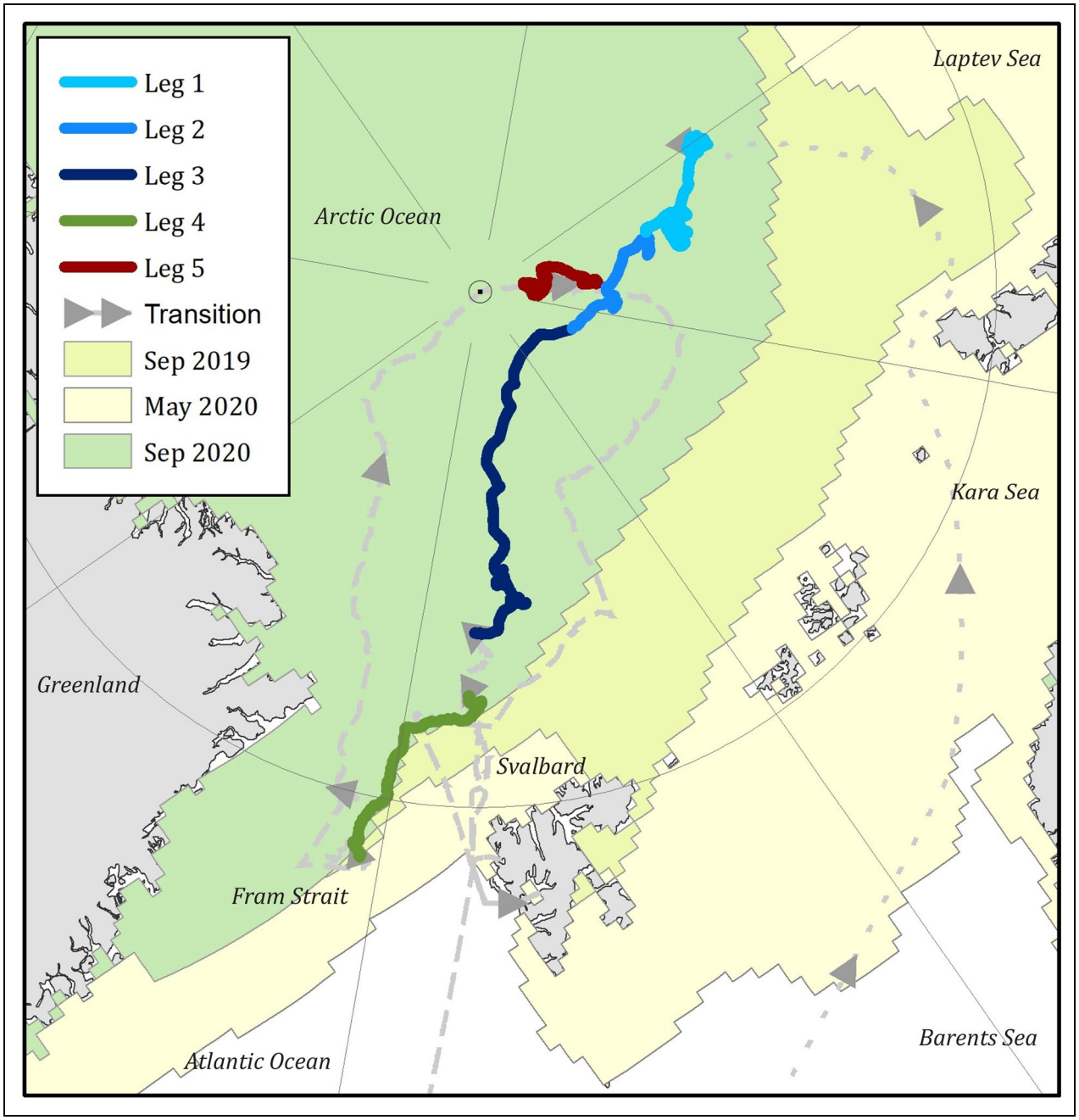

Figure 1. Tracking the drift: MOSAiC expedition 2019–2020. Color-coded tracks depict the 5 legs of the expedition: Leg 1 (October 4, 2019, to December 13, 2019; pale blue), Leg 2 (December 14, 2019, to February 24, 2020; blue), Leg 3 (February 25, 2020, to May 15, 2020; dark blue), Leg 4 (June 17, 2020, to July 31, 2020; green), and Leg 5 (August 12, 2020, to October 12, 2020; brick red). The dotted grey line shows the icebreaker's path during the transition periods between legs, and arrows indicate the direction. The background shows the sea-ice extent at the beginning of MOSAiC (September 2019), at its minimum (September 2020), and its maximum (March 2020) in shades of light green.

legs (**Figure 1**). On September 20, 2019, *Polarstern* left Tromsø and reached its destination on the selected ice floe, north of the Laptev Sea (85°N, 136°E), where the ship was anchored to an ice floe on October 4, and later became frozen into the sea ice. Until May 2020, the selected ice floe remained mostly intact while moving with the TPD across the central Arctic toward Fram Strait (during Legs 1–3; **Figure 1**). From mid-May to mid-June 2020, *Polarstern* temporarily left the original ice floe, transited to Svalbard and back, and reached the edge of the sea ice in Fram Strait on July 31 (78.9°N, 2°E). During Leg 3, *Polarstern* was carried across the Arctic faster than anticipated. Hence, during Leg 5, the ship returned north, to a position near the North Pole (87.7°N, 104°E), where additional measurements were carried out in the central Arctic during the summer (Krumpen et al., 2021). Throughout the entire campaign, observational activities were performed onboard in the proximity of *Polarstern,* in

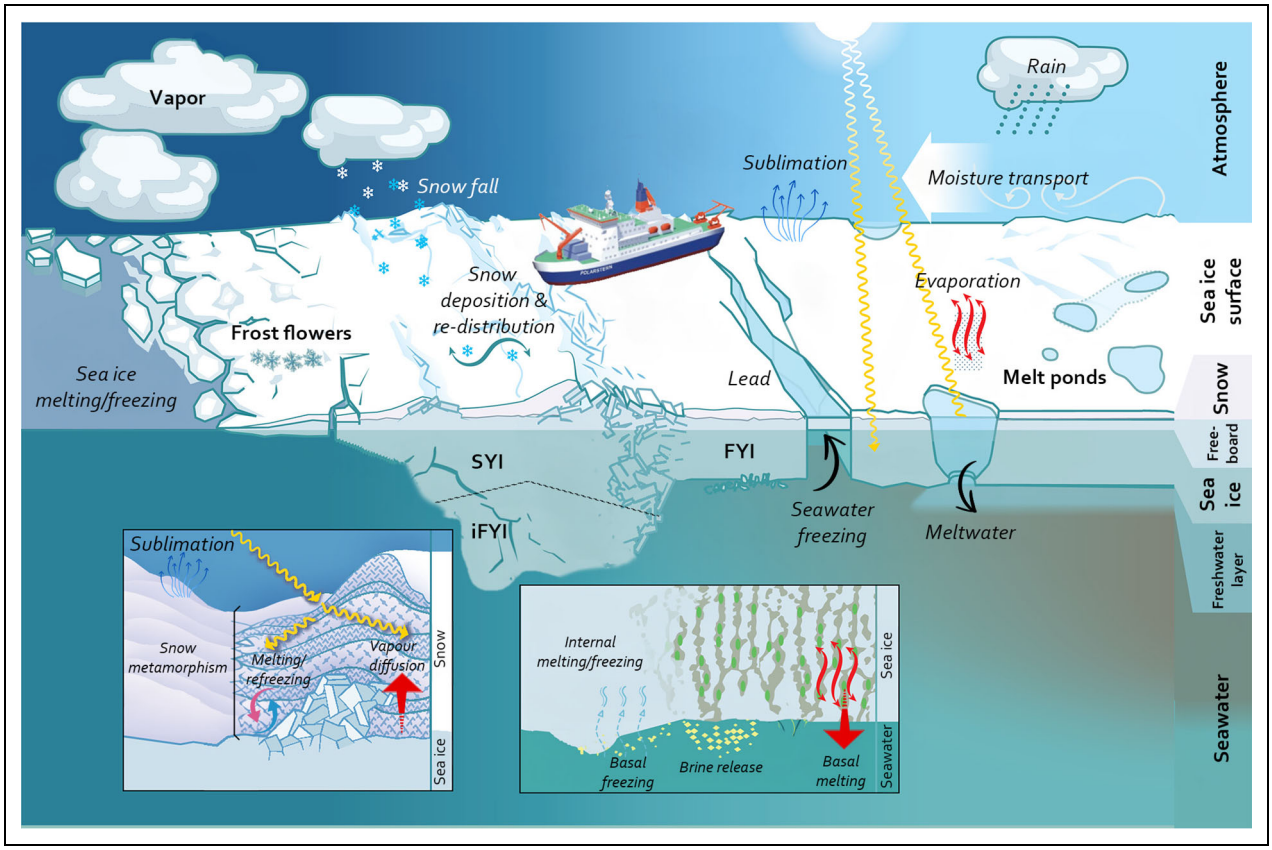

Figure 2. Arctic water cycle components and interactions. Schematic representation of the MOSAiC main ice floe and components of the Arctic water cycle. The diagram illustrates the key components of the Arctic water cycle from which samples were collected during the MOSAiC expedition, including seawater, sea ice, snow, frost flowers, leads, melt ponds, and water vapor. The figure also highlights major exchange and fractionation processes between these components, such as melting, freezing, and sublimation. Depicted forms of sea ice are first-year ice (FYI), insulated first-year ice (iFYI), and second-year ice (SYI). This illustration is a modified version of figure 4 in the MOSAiC overview by Nicolaus et al. (2022).

a Central Observatory ice camp and across a Distributed Network of autonomous observing systems. Moreover, in-situ observations were complemented by coordinated satellite and aircraft observations. The master track of *Polarstern* during the MOSAiC expedition was extracted from the PANGAEA repository (Haas, 2020; Kanzow, 2020; Rex, 2020, 2021a, 2021b).

2.2. Discrete samples

Discrete samples of the different hydrological components (e.g., snow, sea ice, seawater, leads, melt ponds, **Figure 2**) were collected during all legs of the MOSAiC expedition. More than 2200 samples were analyzed for their isotopic ($\delta^{18}O$, $\delta^{2}H$) composition. However, certain limitations in the sampling process during this extensive campaign must be acknowledged. The collection of precipitation samples posed significant challenges due to consistently high wind speeds, which made recognizing snowfall events and collecting samples difficult. Additionally, the diverse teams and individuals involved in collecting seawater, sea ice, and snow samples worked across various locations on the ice floe, introducing complexities in comparing samples and maintaining uniformity in collection methods. Interruptions in sampling occurred periodically due to safety concerns or adverse conditions on the ice floe, which affected the regularity of data collection at certain locations.

2.2.1. Snow and frost flowers

Samples of snow deposited on the sea ice were collected by the snow pit team (Nicolaus et al., 2022) during Legs 1–5 (N = 306) from different locations and sites (i.e., Snow2-A2 and Snow2-A8) in the Central Observatory. Each sample consisted of 3–6 cm of snow collected throughout the vertical snow profile. Snow was typically sampled at 3 different depths (hereafter referred to as bottom, middle, and surface samples). The bottom layer was defined as the snow laying directly above the ice surface, while the surface layer was defined as the surface snow in contact with the air. The middle layer was collected approximately at half the height of the snow profile. The depths of the individual samples in the snow profiles were variable, as the thickness of the snow cover varied spatially and temporally. Snow samples were collected by shovel and were kept frozen in sampling bags until they arrived in the laboratory, where they were thawed at room temperature before analysis. In addition to snow, 10 frost

flower samples were collected opportunistically during Legs 1–3, transferred to gas-tight Tedlar™ bags, melted, and stored in narrow neck bottles at 4°C before analysis.

2.2.2. Sea ice

Sea-ice cores were collected from different sites in the Central Observatory. Level sea ice on the floe was categorized into three types based on age: sea ice that grew during the same winter, referred to as first-year ice (FYI); sea ice that had survived one summer melting period, referred to as second-year ice (SYI); and the new sea ice growing at the bottom of the SYI layer from the freezing of the seawater, referred to as insulated first-year ice (iFYI; Angelopoulos et al., 2022). Some samples were also collected from false bottoms and sea-ice ridges and are presented elsewhere (Smith et al., 2022; Salganik et al., 2023).

Sea-ice cores were collected using a Kovacs Mark II 9 cm diameter corer. The core was extracted and placed in a cradle equipped with a metric ruler. Using a standard Kovacs ice thickness gauge, the freeboard was taken and the length of the core was measured (Angelopoulos et al., 2022). The snow on top of the sea ice was brushed off the top of the cores to minimize snow affecting the ice surface. Due to the harsh winter conditions, cutting and sampling the cores in the field was not feasible. Instead, the cores were transported horizontally to a shipboard laboratory where the temperature was maintained at –20°C. Onboard *Polarstern*, the cores were cut into 10 (Legs 1–3) and 5 (Leg 4) cm sections within the next 30 minutes to 48 hours in the cold room by hand (Leg 1) or using an electric band saw (Legs 2–4). Each section was transferred into a gas-tight Tedlar™ bag. The closed bags were degassed carefully with a vacuum pump (KNF Neuberger, type N035). Melting occurred within 12–15 hours at 4°C. After shaking the melted ice within the Tedlar™ bags, discrete sampling started by first drawing the melt-water upward through a Tygon tube connected with the opened valves of the gas-tight bags and then delivering it into prepared brown narrow-neck 50 ml glass vials. The sea-ice dataset consists of 1043 samples, with 339 from Leg 1, 128 from Leg 2, 328 from Leg 3, 209 from Leg 4, and 39 from Leg 5.

2.2.3. Seawater

On a daily basis, seawater samples were obtained from beneath the keel of the *Polarstern* via a valve system connected to a pump situated at a maximum depth of 10 m below sea level. To avoid contamination, the inlet was kept open for 2 minutes to rinse the pipe thoroughly before the water sample was filled into a 50 ml glass screw cap, sealed, and stored at 4°C before being transferred to the laboratory for isotope analysis. Salinity was not measured directly at the time of collection. Instead, salinity values were obtained at 1 h resolution from the ship-based conductivity-temperature profiling through depth (CTD) sensors (Tippenhauer et al., 2021); daily averages were calculated and attributed to the seawater isotopic measurements. In this study, salinity is reported on the practical salinity scale. The resulting "underway seawater" dataset consists of 302 continuous observations from November 2019 to October 2020 (Mellat et al., 2022b).

Additional seawater samples were obtained during Legs 1–3 of the expedition at the site called Ocean City (OC) (Rabe et al., 2022), from here on referred to as the "OC seawater" dataset. Seawater profiles were collected from the ice floe once a week at variable depths. A 12-bottle CTD rosette was used for water sampling from the sea surface to the ocean bottom, and water from the Niskin bottles at each water depth was sampled. This study presents the results from 43 surface samples (from 2–5 m depth). Storage and transport were identical to the "underway seawater" samples.

2.2.4. Leads and melt ponds

Two types of lead samples were collected and are presented in this work. During Legs 1–3, ice samples were obtained from refrozen leads using an ice saw or ice corer, while during Legs 4 and 5, the surface layer of water from open leads surrounding *Polarstern* was collected. In total, 137 samples were taken from leads, from which 80 were lead ice and 57 were lead water. In addition, water samples from melt ponds surrounding *Polarstern* were collected. Our dataset includes 109 samples collected from melt ponds, during Legs 4 and 5.

2.3. Stable water isotope analysis

All discrete water samples presented here from the MOSAiC expedition were stored at 4°C before being analyzed for stable water isotopes at the ISOLAB facility of the AWI in Potsdam, Germany. The isotope composition ($\delta^{18}O$ and $\delta^{2}H$) was determined using a Finnigan MAT Delta-S mass spectrometer fitted with two equilibrium units following a procedure described in Meyer et al. (2000). The $\delta^{18}O$ and $\delta^{2}H$ values are expressed as parts per mil deviation from the V-SMOW standard. For estimating the accuracy of the measurements, a quality control standard (HDW) was used, yielding a mean and standard deviation (SD) of $-12.6‰ \pm 0.1‰$ ($N = 54$) and of $-95.3‰ \pm 0.6‰$ for $\delta^{18}O$ and $\delta^{2}H$, respectively.

3. Results and discussion

The statistical summary of the isotopic composition of all discrete samples from different components of the Arctic water cycle is presented in **Table 1** and **Figure 3**. The dataset exhibits a range of $\delta^{18}O$ values from –39.6‰ for snow to 1.4‰ for iFYI. Meanwhile, the *d-excess* values vary between a minimum of –26.6‰ and a maximum of 26.5‰, both for snow. A more detailed analysis of the isotope measurements for snow, sea ice, seawater, and the interactions between different components is presented in the following subsections.

3.1. Snow

3.1.1. Isotopic measurements of snow

Snow samples were collected from different locations on the MOSAiC ice floe to analyze the variability of $\delta^{18}O$, $\delta^{2}H$, and *d-excess* values. In general, snow had the most $\delta^{18}O$-depleted isotope signatures of all hydrological

Table 1. Statistical overview of water isotope measurements collected during the MOSAiC expedition

		$\delta^{18}O$ (‰)				$\delta^{2}H$ (‰)				*d-excess* (‰)				Co-isotope Relationship		
Sample Type[a]	***N***	**Min**	**Mean**	**Max**	**SD**[b]	**Min**	**Mean**	**Max**	**SD**	**Min**	**Mean**	**Max**	**SD**	**Slope**	**Intercept**	**R^2**
OC seawater	*43*	−2.72	−1.69	−0.45	0.67	−17.9	−11.6	−2.4	4.8	−1.6	2	5.2	1	7.09	0.42	0.97
Underway seawater	*302*	−3.44	−1.55	0.36	0.88	−26	−11.2	2.5	6.7	−1.1	1.2	3.5	0.8	7.6	0.59	0.98
Lead water	*57*	−7.84	−2.31	1.33	1.7	−68.1	−17.5	10.2	12.9	−7.7	1	5.8	2.5	7.46	−0.27	0.96
Snow	*306*	−39.63	−16.26	−0.64	9.06	−304.9	−123.5	−4.7	66.3	−26.6	6.6	26.5	9.3	7.28	−5.02	0.99
Frost flowers	*10*	−31.12	−9.55	−2.71	9.35	−235	−69.1	−20.8	69.7	−2.9	7.3	19.3	7.7	7.43	1.86	0.99
FYI	*631*	−17.45	−0.73	1.6	2.08	−132.2	−5.4	12.2	16.1	−4.1	0.5	7.4	1.1	7.72	0.27	0.99
SYI	*311*	−10.69	−4.48	0.82	2.21	−82.4	−34.3	5.7	17	−1.3	1.5	5.9	1.1	7.66	0.05	0.99
iFYI	*107*	−2.6	0.2	1.44	0.66	−19.4	2	12.2	5.1	−1.3	0.4	4.8	0.8	7.61	0.49	0.97
Lead ice	*80*	−17	−1.18	1.36	2.67	−120.5	−8.2	11.2	19.4	−1.5	1.2	15.1	2.2	7.26	0.37	0.99
Melt ponds	*109*	−12.59	−2.05	0.94	2.69	−93.3	−15.5	8	20.4	−2.7	0.9	7.4	1.6	5.57	−0.01	0.99

[a] Seawater from site Ocean City (OC seawater), first-year ice (FYI), second-year ice (SYI), insulated first-year ice (iFYI).

[b] Standard deviation.

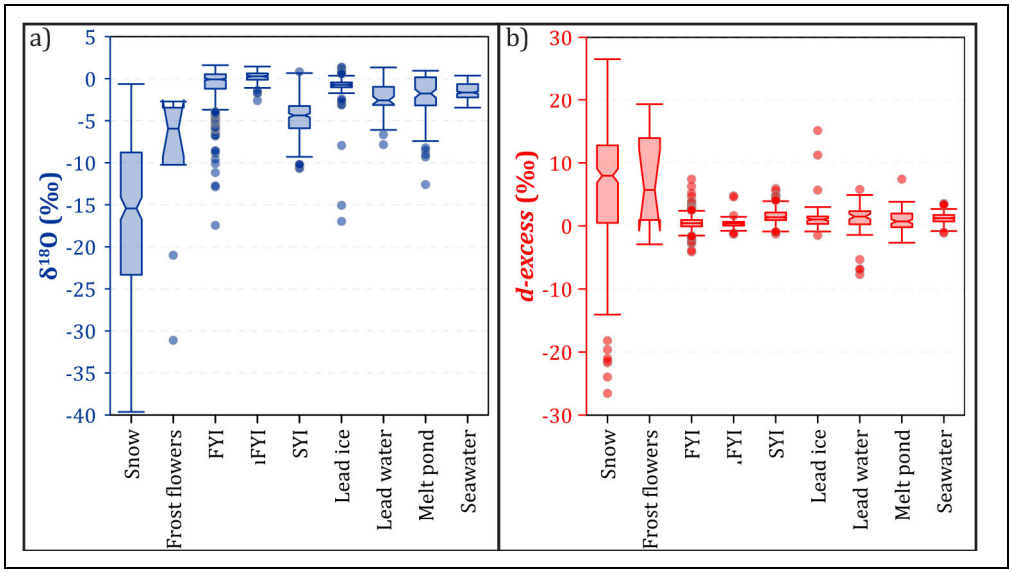

Figure 3. Statistical distribution of the isotopic measurements. Distribution of (a) $\delta^{18}O$ (‰) and (b) *d-excess* (‰) measured on the various sample types collected. Values measured by interquartile range test are shown as boxplots, where horizontal lines within each box represent the median of the dataset, whiskers on boxes show the highest and lowest values within 1.5 times the interquartile range from the upper and lower quartiles, and dots outside the whiskers represent the outliers. Forms of sea ice sampled are first-year ice (FYI), insulated first-year ice (iFYI), and second-year ice (SYI).

components, with mean $\delta^{18}O$ and $\delta^{2}H$ values of –16.3‰ and –123.5‰, respectively. Moreover, snow also had the widest range of $\delta^{18}O$ values (–0.6‰ to –39.6‰, N = 306; **Table 1**; **Figure 3a**). Frost flowers were the second-most $\delta^{18}O$-depleted hydrological component, with a mean $\delta^{18}O$ of –9.55‰ and the highest SD (9.4‰), similar to the SD of snow (9.0‰). Snow and frost flower samples were characterized by high mean *d-excess* values of 7.3‰ and 6.6‰, respectively. However, the most negative *d-excess* values were also observed among snow samples (–26.6‰; **Figure 3b**).

On average, the $\delta^{18}O$ values in the snow displayed an increasing trend from the top layer (–22.5‰ ± 6.7‰; N = 98) to the middle layer (–17.3‰ ± 8.2‰; N = 73) to the bottom layer (–9.7‰ ± 6.1‰; N = 92; as shown in **Table 2**). This trend corresponds to a 5.2‰ increase in $\delta^{18}O$ between the surface and middle layers and another 7.6‰ offset between the middle and bottom layers. The $\delta^{18}O$-$\delta^{2}H$ linear regressions exhibited distinct slopes and intercepts for the top ($\delta^{2}H = 7.9 * \delta^{18}O + 11.1$), middle ($\delta^{2}H = 7.4 * \delta^{18}O - 1.7$), and bottom layers ($\delta^{2}H = 7.0 * \delta^{18}O - 11.0$; **Table 2**). The slope of the top layer (7.89) was slightly lower than the GMWL slope (8.00), while the slopes of the middle (7.4) and bottom layers (7.0) were considerably lower than the GMWL slope. Hence, the change of the isotopic composition with depth is accompanied by a decrease in slope and intercept from top to bottom. This decrease indicates that the isotopic composition of snow in the study area deviates from the GMWL and that this relationship depends on the height of the snow profile, indicating that there are secondary processes (i.e., sublimation, vapor diffusion within the snowpack) underway in the snowpack (Ala-aho, 2021).

Opposite to the $\delta^{18}O$ signal, the *d-excess* values decreased from the top to the bottom layer of snow (**Figure 4**). Comparing the mean values and SDs, we observed that snow from the top layer had the highest mean *d-excess* value (13.4‰) and the lowest SD (5.4‰). In contrast, snow at the bottom had the lowest mean *d-excess* value (−1.7‰) and the highest SD (8.9‰), indicating a higher variability in the values with increasing depth. Snow in the middle fell between these two, with an intermediate mean *d-excess* value of 8.3‰ and SD of 6.9‰.

Given the physical proximity between snow and sea ice, the results of the isotope composition of the surface sea-ice samples were analyzed together with the snow (**Figure 4**). The top 5–10 cm of sea ice exhibited a relatively constant mean $\delta^{18}O$ of −4.4‰ ± 3.5‰ (N = 93) throughout the sampling period with a low SD (1.9‰), indicating relatively consistent values across this sample set. Hence, the surface layer of sea ice was, on average, 5.4‰ more enriched in ^{18}O than the bottom layer of snow. Compared to FYI and ocean water samples, however, the surface layer of sea ice had a lower $\delta^{18}O$ value (**Table 1**).

Figure 5 presents a time series spanning October 2019 to July 2020, depicting weekly averaged air temperatures and surface snow $\delta^{18}O$ values, which suggests a relationship between these variables. The cyclic patterns in the upper and middle snow layers showcase lower $\delta^{18}O$ values (−40‰ to −10‰) in January and February 2020 (Leg 2) and higher values (−27‰ to 5‰) from October to December 2019 (Leg 1). Interestingly, the lowest $\delta^{18}O$ values (−25‰ to −15‰) in the bottom snow layer correspond to the June–August 2020 period (Leg 4), contrasting with the highest $\delta^{18}O$ values aligning with Leg 2. These

Table 2. Statistical overview of water isotope measurements of snow samples collected during the MOSAiC expedition compared to the sea-ice surface

			$\delta^{18}O$ (‰)				$\delta^{2}H$ (‰)				*d-excess* (‰)				Co-isotope Relationship		
Sample Type	***N***	**Mean Depth (cm)**	**Min**	**Mean**	**Max**	**SD[a]**	**Min**	**Mean**	**Max**	**SD**	**Min**	**Mean**	**Max**	**SD**	**Slope**	**Intercept**	**R^2**
Snow top	*98*	20.1	−39.63	−22.48	−3.57	6.66	−304.9	−166.4	−30.0	52.8	−1.8	13.4	26.5	5.4	7.89	11.09	0.99
Snow middle	*73*	14.8	−37.14	−17.27	−3.88	8.19	−277.8	−129.9	−37.1	60.9	−6.1	8.3	23.4	6.9	7.42	−1.74	0.99
Snow bottom	*92*	8.3	−26.10	−9.71	−1.45	6.12	−197.2	−79.4	−16.1	43.6	−26.6	−1.7	16.0	8.9	7.04	−11.02	0.99
Sea-ice top	*93*	[b]	−17.45	−4.40	0.84	3.49	−132.2	−34.4	6.9	26.5	−4.1	0.8	7.4	1.9	7.59	−0.95	0.99

[a] Standard deviation.

[b] 5–10 cm from the surface of the ice.

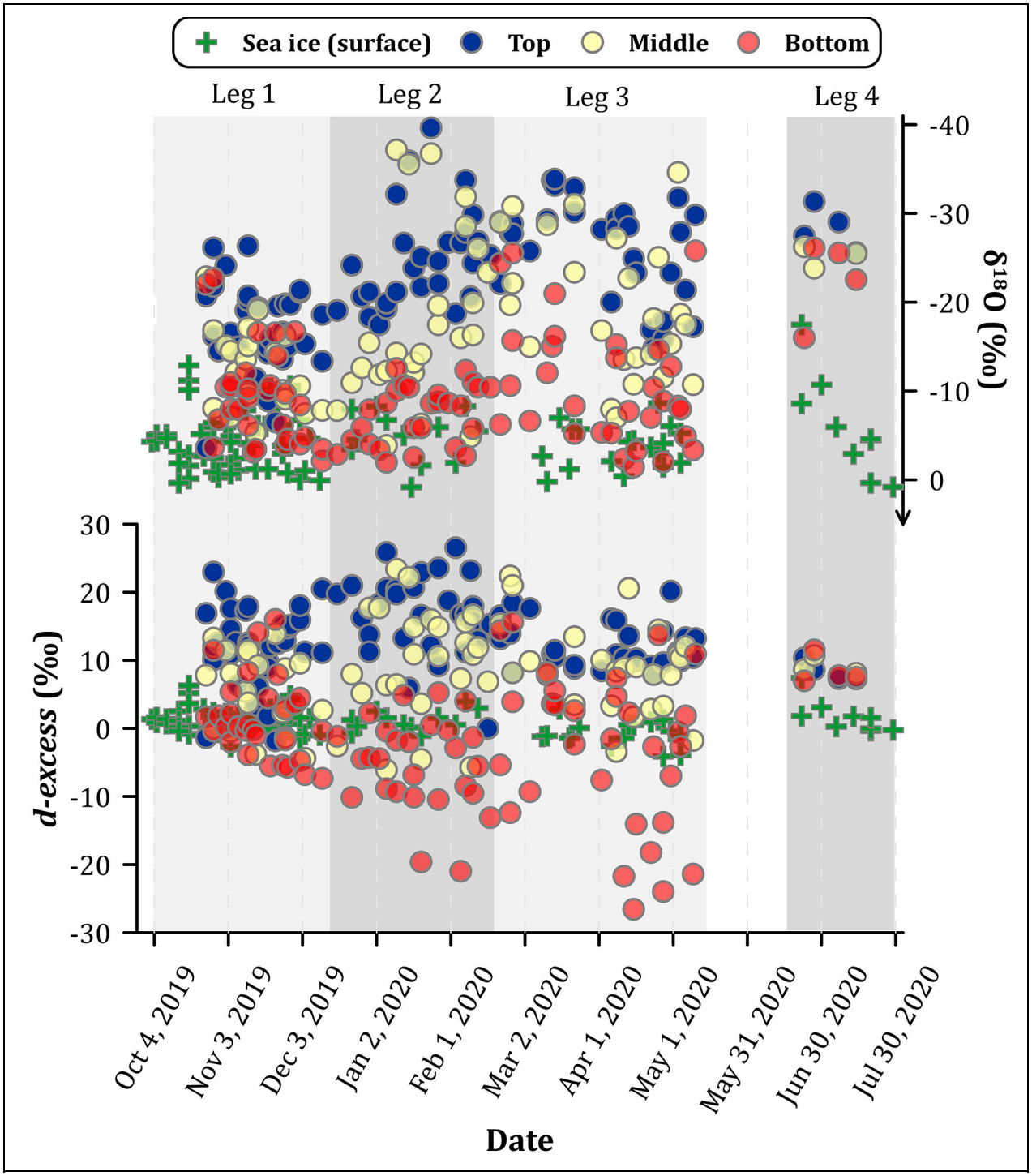

Figure 4. Time series of snow isotopes at different layers and surface sea ice. Time series of $\delta^{18}O$ (upper panel) and *d-excess* (lower panel) measurements of snow samples collected during MOSAiC in three layers (top, blue; middle, yellow; bottom, red), and sea ice at the surface (upper 5–10 cm, green). The $\delta^{18}O$ axis is reversed to better represent the surface-to-bottom change of values in snow profiles. The sampling periods of Legs 1–4 are shown on the time series as shaded backgrounds.

findings underscore the role of temperature as a primary driver of seasonal isotopic shifts, a concept initially introduced by Dansgaard (1964).

The Arctic Ocean receives most of its precipitation from the Atlantic and Pacific Oceans, as well as from ice-free areas within the Arctic Ocean itself. Throughout each season, a combination of factors including temperature, humidity, and air mass trajectories influence the isotopic characteristics of snow, supporting previous findings (Mellat et al., 2021). While the overall trajectory of mean $\delta^{18}O$ in the upper snow surface samples mirrors air temperature fluctuations during winter, a closer examination reveals intricate dynamics. However, a direct and statistically significant correlation between the daily isotopic

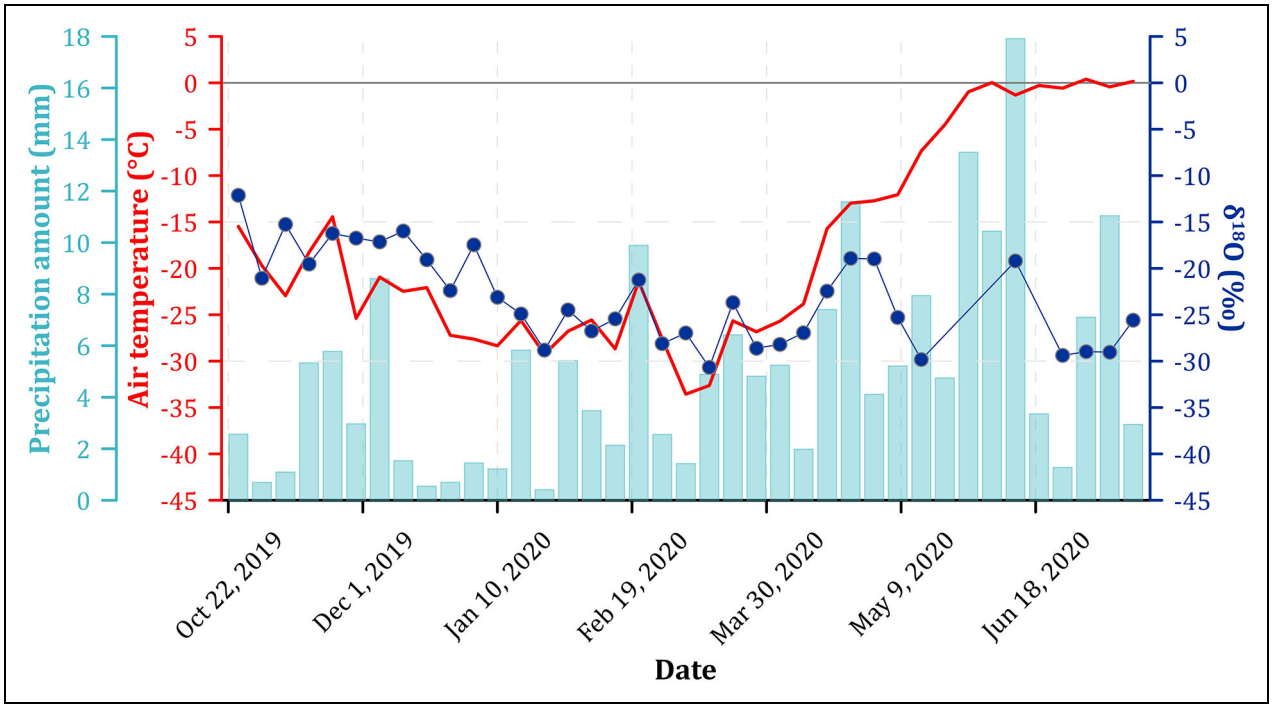

Figure 5. Surface snow isotopes throughout MOSAiC. Time series of weekly averaged air temperature (red) and surface snow $\delta^{18}O$ (dark blue) from October 2019 to July 2020. The aggregated weekly precipitation amount (mm) along the track of *Polarstern* extracted from the global analysis is presented as the light blue line (Hersbach et al., 2020).

composition of surface snow samples and concurrent daily air temperatures does not exist (Figure S1). The correlation coefficient between these variables is notably low, indicating a complex interplay (slope = 0.04, R^2 = 0.02). This divergence is particularly evident in April 2020, as highlighted in **Figure 5**. However, the relationship between air temperature and surface snow $\delta^{18}O$ values shows a subtle yet noticeable upward trend from September 2019 to April 2020 (slope = 0.47, R^2 = 0.13, *p*-value = 0.04).

More detailed time series of snow isotope profiles sampled at two sites (Snow2-A2 and Snow2-A8; Figure S2) are provided in **Figure 6**. They exhibit similar patterns in both $\delta^{18}O$ and *d-excess* values across the three layers of snow (**Figure 6a**, **b**). The changes in $\delta^{18}O$ observed in the top layer of snow at both stations could be linked to the changes in snow depth (up to 38 cm), as the snow became increasingly depleted in $\delta^{18}O$ with each increase in depth. Notably, *d-excess* values lower than −15‰ were observed primarily at the snow2-A2 site (**Figure 6a**), where a negative trend from −9.3‰ to −26.6‰ is obvious between January 10, 2020, and April 15, 2020 (also visible in **Figure 4**). This continuous change in the *d-excess* values from Leg 1 until the end of Leg 4 was most pronounced in the bottom layer of the snow that is in contact with the sea ice, due to vapor transport during snow metamorphism (Sturm et al., 1997).

3.1.2. What defines the snow isotopic composition on the sea ice in the central Arctic?

The mean $\delta^{18}O$ values showed a gradual increase of approximately 13‰ from the surface down to the bottom of snow profiles. Correspondingly, there was a 12‰ decrease in *d-excess* as one moved toward the base of the snow profiles. This pattern becomes evident when contrasting the $\delta^{18}O$ and *d-excess* values of the surface snow with those found in the middle and bottom layers. This consistency in findings supports the conventional composition of the surface snow samples, where fresh snowfall typically exhibits lower $\delta^{18}O$ and higher *d-excess* values. This alignment makes sense considering that the introduction of new snow through precipitation significantly influences the overall isotopic composition of the snow cover (Ala-aho et al., 2021). The factors affecting isotopic compositions in snow are well-captured in the work by Stichler et al. (1981), which underscores the influence of temperature, air moisture, and air mass origin on the precipitation isotopes. These variables collectively give rise to the observed seasonal variation in heavy isotope concentrations in precipitation, with higher values during summer and lower values during winter. The high *d-excess* values at the snow surface support this hypothesis. The correlation of $\delta^{18}O$ changes in top layer snow with snow depth changes (**Figure 5**) also suggests that these isotopic changes were caused by added snow at the surface, for example, by precipitation or wind drift, and is supported by findings of Zuhr et al. (2023). However, the weak to non-existing correlation between surface temperatures, precipitation amounts, and the isotopic values of the top snow layers (**Figure 4**) indicate that the contribution of meteoric waters (e.g., fresh snowfall) was either very limited or that snow undergoes metamorphism after deposition. Such isotopic changes of the top snow layer by

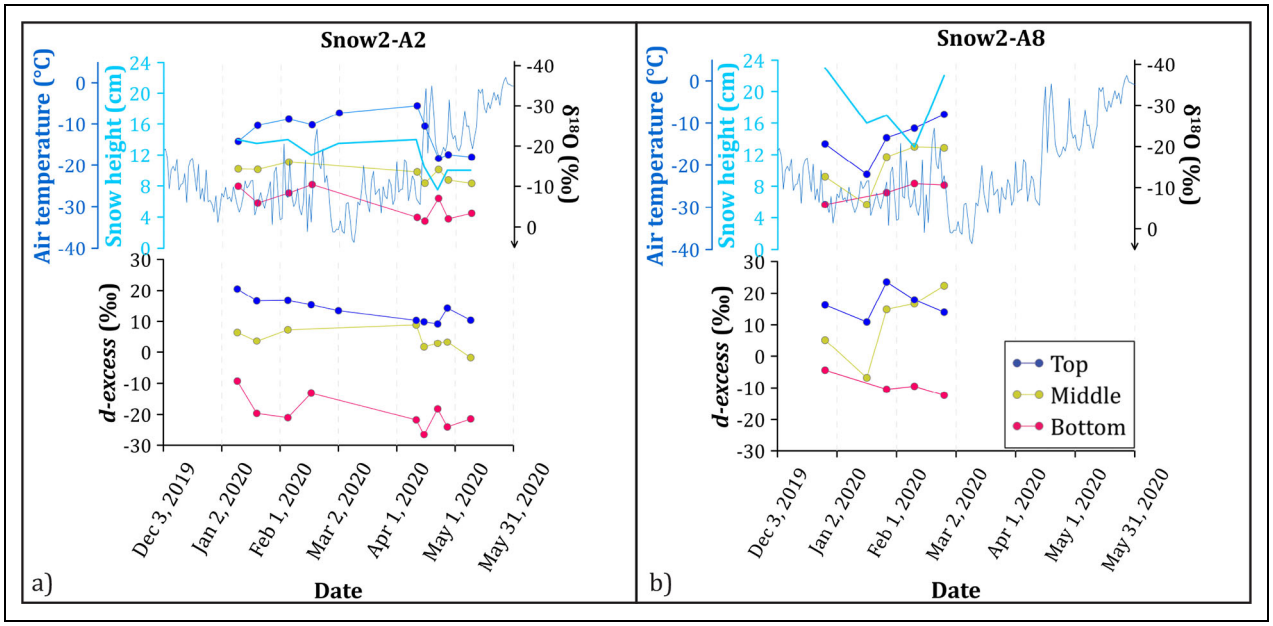

Figure 6. Time series of $\delta^{18}O$ and *d-excess* at two snow sampling sites. Both sites (a) Snow2-A2 and (b) Snow2-A8 had snow located on top of second-year ice. Snow height for each sample and average daily air temperature data (Schmithüsen, 2021a) are shown as secondary y-axes. The top layer of snow samples is presented as dark blue circles, the middle layer as yellow circles, and the bottom layer as red circles.

postdepositional sublimation have recently been suggested by Wahl et al. (2021) and cannot be excluded from our samples. To quantify the impact of fresh snowfall on the isotopic composition of the snowpack and the influence or absence of post-depositional sublimation effects, a higher resolution event-based snow sampling is required. Unfortunately, such sampling was not performed during the MOSAiC campaign.

The process of vapor sublimation and vertical diffusion can take place between the relatively warmer sea-ice surface and the comparatively colder overlying snow layer (Jafari et al., 2020). As a consequence of this sublimation, water vapor originating from the sea ice tends to possess a higher $\delta^{18}O$ in comparison to the snow cover above it (refer to **Table 1** and **Figure 3**). This phenomenon has the potential to lead to an enrichment of $\delta^{18}O$ within the snow through metamorphism. The subsequently enriched isotopic signature of vapor can then be transported upward within the snowpack along the thermal gradient, facilitated by additional vapor advection as explained by Sommerfeld et al. (1991) and Stichler et al. (1981) and upward movement within the snow layer as described by Friedman et al. (1991). Vertical vapor transport helps to explain the consistent isotope gradient observable in snow profiles.

The Arctic region's snowpack undergoes substantial temperature variations with time, particularly notable during winter, due to the marked differences between air and ocean temperatures. This climatic characteristic leads to the development of recrystallization processes and the formation of columnar snow structures, known as depth hoar (Pinzer et al., 2012). These features were noted frequently during the MOSAiC expedition (Nicolaus et al., 2022). A reasonable assumption is that the vertical isotopic changes within the sea ice's snow cover are closely interconnected with these observed recrystallization effects. During the summer months, vapor sublimation from the sea ice is suppressed due to the isothermal temperature.

Compared to the top snow layer, the middle and bottom layers of the snow profiles show higher $\delta^{18}O$ and lower *d-excess* values, which may be linked with postdepositional snow metamorphic processes. These observations during MOSAiC are similar to other snowpack isotope studies in the Arctic, with variation from the surface to the bottom layers (Ala-aho, 2021). For instance, in Alaskan tundra snowpack, profiles of $\delta^{18}O$ values for the most recent storm were recognizable; however, postdepositional processes modified the remaining isotope profiles from near the top to the bottom of the snowpack. In comparison, in taiga snowpack $\delta^{18}O$ profiles in the eastern Arctic, where there is significantly less wind-driven redistribution than in the open Alaskan tundra, layering and preservation of divergent moisture sources and isotopic memory were much more apparent. Snow metamorphism involves both sublimation and recrystallization, which can cause changes in the isotopic composition of snow, leading to the further enrichment of heavy isotopes in the remaining snow (Friedman et al., 1991; Ebner et al., 2017; Wahl et al., 2022). Enrichment by sublimation in snow isotopes has also been reported by Steen-Larsen et al. (2014) and Casado et al. (2021), albeit in different environmental settings.

At the bottom boundary of the snow layer, the snow was more depleted in $\delta^{18}O$ values than the underlying sea-ice surface. However, the surface layer of sea ice itself was

also more $\delta^{18}O$-depleted than between FYI and ocean water samples. These isotopic differences together suggest that an additional isotopic exchange between the bottom layer of snow and the sea-ice surface layer occurred and that this exchange altered both the bottom snow and sea-ice surface layer samples.

Besides sublimation and diffusion processes, changes in the vertical isotopic composition of the snow layer might be caused by the partial melting of snow, especially when temperatures are close to the melting point. When the snow melts, the lighter isotopes of oxygen are more likely to diffuse into the vapor phase, leading to the remaining snow becoming slightly enriched in its $\delta^{18}O$ values (Beria et al., 2018; Aemisegger et al., 2022). However, in the context of MOSAiC, the possibility of melting, percolation, and refreezing of snow was unlikely due to continuously negative temperatures during Legs 1–3. This interpretation was additionally supported by the absence of ice layers in the individual snow profiles, which would be indicative of melting and refreezing. However, during Leg 4, a partial melting of snow occurred, which could be responsible for the more uniform isotope composition between the different layers of snow due to percolation of meltwater through the snowpack.

In summary, the isotopic gradients observed in snow profiles from Legs 1–3 of the MOSAiC expedition result from the complex interplay of various processes. These processes differ for each profile and depend on factors like air temperature, wind, and sea-ice type beneath the snowpack. Notably, the dominant influences on the lower snowpack in the central Arctic are the mixing of material from the sea-ice boundary and moisture transfer from the ocean. These effects overprint interactions at the snow-atmosphere interface, such as precipitation and wind-driven snow accumulation. The findings of this study align with a similar dataset and analysis (AR Macfarlane, unpublished data), which delves deeper into snow and sea-ice metamorphism processes during MOSAiC.

3.2. Sea ice

3.2.1. Isotopic composition of sea ice

The different types of sea ice that were measured had distinctly different $\delta^{18}O$ values (**Table 1**). FYI had a mean $\delta^{18}O$ value of -0.7‰ and was isotopically more enriched compared to SYI ($\delta^{18}O = -4.6$‰) which, surviving one melt season, had the lowest $\delta^{18}O$ among all sea-ice samples. The mean $\delta^{18}O$ value of 0.2‰ for iFYI was the highest, whereas lead ice $\delta^{18}O$ averaged -1.18‰. Although, the mean *d-excess* values of FYI and iFYI were similar at 0.5‰ and 0.4‰, respectively, SYI had a slightly higher *d-excess* of 1.6‰.

The main coring sites (MCS) were established on first-year ice (MCS-FYI) and second-year ice (MCS-SYI), where coring activities were conducted from late October 2019 until the end of Leg 3 in May 2020 (Angelopoulos et al., 2022). To gain a better understanding of the temporal sea-ice development, **Figure 7** presents the combined data of salinity and $\delta^{18}O$ at the MCS-FYI and MCS-SYI sites. These data allow a more detailed consideration of sea-ice isotope variability. At the MCS-FYI site, the $\delta^{18}O$ values exhibited a broad range from -6.7‰ to 1.6‰, with a mean value of -0.2‰ $\pm$ 1.4‰. At the MCS-SYI, the $\delta^{18}O$ values fluctuated between -8.0‰ and 1.4‰, with a mean value of -2.8‰ $\pm$ 2.3‰. Salinity at MCS-FYI varied widely, ranging from 2.1 to 14.9, with a mean value of 5.2 $\pm$ 1.4, whereas MCS-SYI showed a smaller range of variation, with salinity levels between 0 and 7.5, and a mean value of 2.1 $\pm$ 2.0 (**Figure 7**). Generally, the MCS-FYI $\delta^{18}O$ values were distributed mainly around 0‰. However, near the surface, that is, above 20–30 cm, distinctly lower $\delta^{18}O$ values to about -4‰ were observed. These lower values were accompanied by a slight increase in salinity (**Figure 7**). MCS-SYI $\delta^{18}O$ values were also lowest near the surface but showed an increase in $\delta^{18}O$ toward greater depth, which was in line with a rise in salinity. Below about 70 cm depth (iFYI, **Figure 8a**, **b**), some of the MCS-SYI cores tend to show an isotope-salinity pattern similar to MCS-FYI. Generally, the MCS-SYI $\delta^{18}O$ and salinity values were much lower to a greater depth. Sea-ice *d-excess* values were distributed mainly around 0.0‰ with some positive and negative deviations, the latter especially for SYI samples.

3.2.2. Sea-ice growth and changes in isotopes

The growth of sea ice in the Arctic Ocean is a complex process (Notz and Worster, 2008) that is influenced by various environmental factors, such as temperature, salinity, wind, and ocean currents. Valuable insights into the formation and evolution of sea ice can be gained by analyzing its isotopic composition (Toyota et al., 2013; Granskog et al., 2017; Tian et al., 2018). As sea ice forms, it extrudes salt, which is then released into the seawater (so-called brine release). The process of freezing is accompanied by isotope fractionation processes also due to diffusion at the ice-water interface (Lehmann and Siegenthaler, 1991), favoring heavier isotopes to remain in the sea ice, whereas lighter isotopes are released to the seawater (Beck and Münnich, 1988). This fractionation results in the depletion of the surface seawater in $\delta^{18}O$ (**Table 1**), indicative of the rate of sea-ice growth as well as of brine release into the ocean (Toyota et al., 2013).

Compared to SYI, FYI was more enriched in heavy isotopes, attributable to multiple factors. One primary distinction is that FYI originated from the freezing of ocean water with a relatively consistent isotopic composition around 0‰ during the MOSAiC expedition (**Table 1**). In contrast, SYI was formed in the Laptev Sea or its vicinity, particularly near the Laptev Sea shelf break (Krumpen et al., 2020). In this region, surface water salinity and $\delta^{18}O$ values are notably lower due to freshwater inputs from surrounding snow-dominated watersheds (Bauch et al., 2009; Bauch et al., 2016; Juhls et al., 2020). Further, SYI has undergone a freeze-thaw cycle, involving the melting of surface snow and subsequent contribution of meltwater into the remaining SYI. This process leads to both lower salinity and lower $\delta^{18}O$.

The isotopic composition of SYI could be influenced by periods of partial melting, further altering its isotopic composition. Additionally, heavy isotopes may be enriched in the pond water due to evaporation from melt

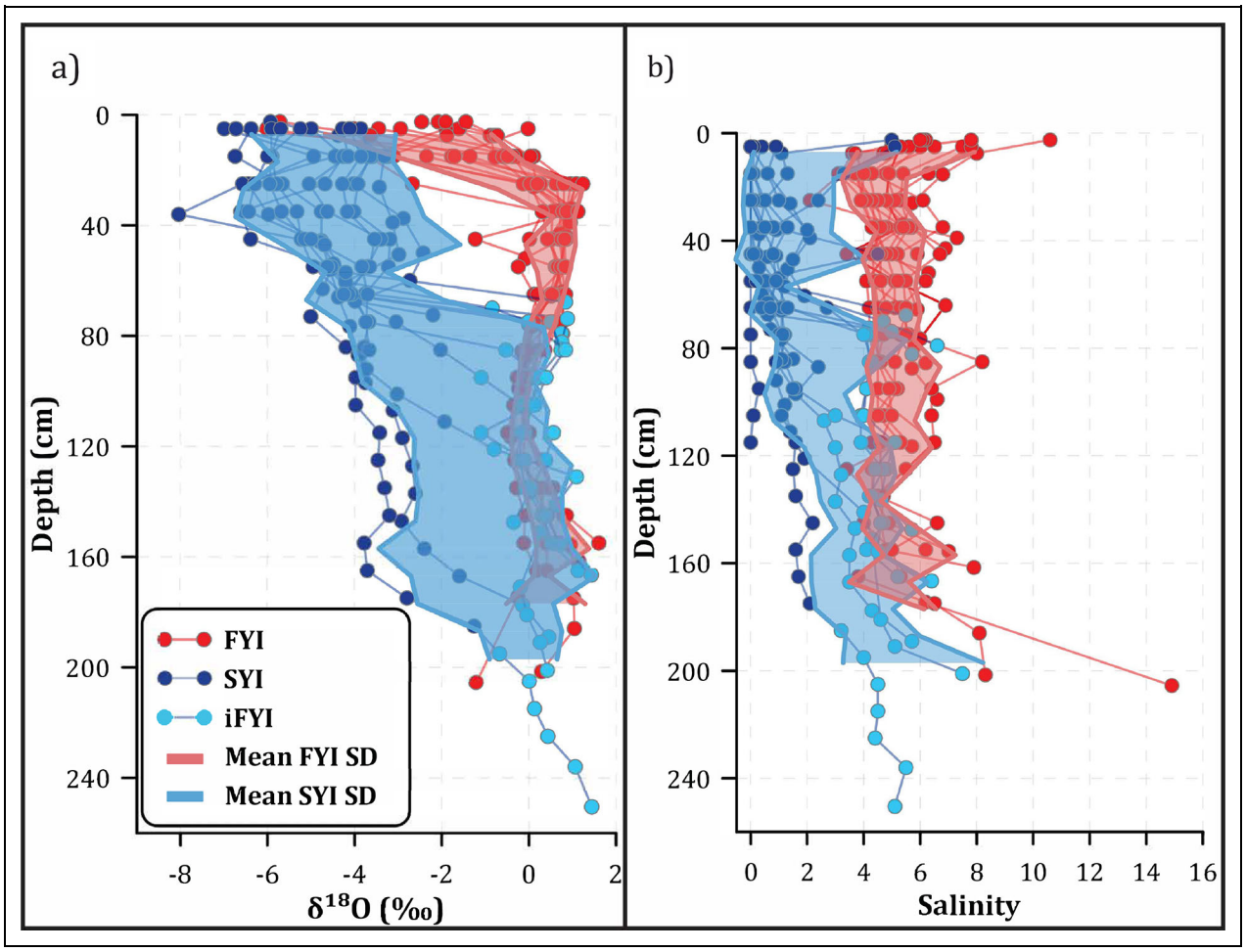

Figure 7. Depth profiles of sea-ice core $\delta^{18}O$ and salinity at sites MCS-FYI and MCS-SYI. Measurements of (a) $\delta^{18}O$ and (b) salinity, where the samples collected at the main coring sites on first-year ice (MCS-FYI) are shown in red circles, and those from the main coring sites on second-year ice (MCS-SYI) are shown in blue circles. The light blue circles represent the insulated first-year ice (iFYI) samples from MCS-SYI. The standard deviations (SD) from calculated mean values of both $\delta^{18}O$ and salinity for FYI samples and SYI including iFYI samples are shown as shades of blue and light red, respectively, on the plots.

ponds. During winter, a newly formed ice layer known as iFYI develops beneath SYI. We follow the terminology presented in Angelopoulos et al. (2022), which slightly deviates from basic sea-ice definitions (World Meteorological Organization, 2014) but facilitates the explanation of our time series. iFYI generally exhibits higher $\delta^{18}O$ values compared to the overlying SYI, influenced by similar factors that are responsible for the heavier isotope composition of FYI compared to SYI. However, iFYI has a slower growth rate than FYI, resulting in less pronounced kinetic fractionation during the freezing process. While SYI might be exposed to the atmosphere and exchange water vapor, the isotopic composition of underlying seawater primarily influences iFYI. Therefore, the isotopic composition of sea ice provides useful information about its formation and can help distinguish between ocean-sourced FYI and iFYI from SYI with a larger meteoric contribution. Our analysis of the isotopic composition of MCS-FYI and MCS-SYI in the Arctic Ocean is supported by earlier findings of studies by Granskog et al. (2017) and Lange et al. (2021). The authors observed that FYI had a higher isotopic composition compared to SYI (**Figure 8a**), concluding on differences in the sources of water for ice formation. Furthermore, our data reveal that the isotopic composition of both SYI and FYI had slightly lower $\delta^{18}O$ toward the surface (**Figure 8a**), which suggests a snow contribution in the upper approximate 20 cm of the FYI cores. For the SYI, the top 70 cm displayed a lighter isotope composition, also reflected in low salinities at MCS-SYI throughout the expedition (**Figure 8b**). At the MCS-SYI site, the iFYI layer had grown at the bottom with slow brine release toward the bottom of the ice (Angelopoulos et al., 2022). The changes in our $\delta^{18}O$ data aligned with the changes in salinity (or brine volume fraction; Angelopoulos et al., 2022) with a threshold of about −2‰ as an indicator for separating the iFYI from the upper SYI layer (**Figure 8b**).

3.3. Seawater

3.3.1. Isotopic composition of surface seawater

OC seawater and underway seawater samples had similar mean $\delta^{18}O$ values of −1.7‰ and −1.5‰, respectively, while lead water samples had a mean $\delta^{18}O$ of −2.3‰.

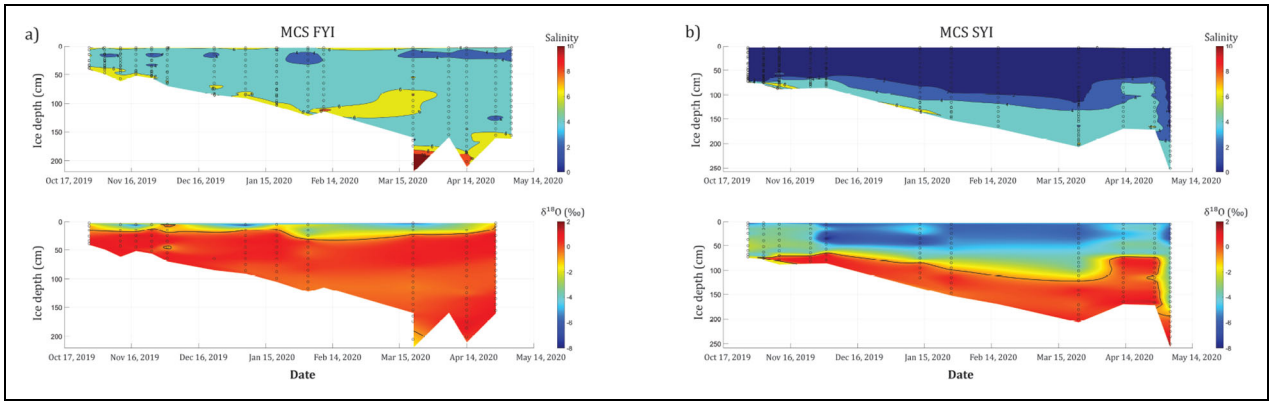

Figure 8. Time series of sea-ice core salinity and $\delta^{18}O$ at sites MCS-FYI and MCS-SYI. Measurements made at (a) the main coring sites on first-year ice (MCS-FYI) and (b) the main coring sites on second-year ice (MCS-SYI). The upper panels illustrate the temporal evolution of salinity (Angelopoulos et al., 2022), while the lower panels depict the changes in $\delta^{18}O$. The data presented are interpolated between sea-ice core retrievals (dashed vertical lines), and the timelines are color-coded according to the corresponding salinity and $\delta^{18}O$ values. A thin black line in the $\delta^{18}O$ panels corresponds to the sharp change in bulk salinity of sea ice and represents the theoretical border line between SYI and insulated first-year ice (iFYI) layers.

These values were associated with mean *d-excess* values of 2.0‰, 1.2‰, and 1.1‰, respectively (**Table 1**). The variability of $\delta^{18}O$ in the underway seawater samples collected during all five legs of the expedition (−3.4‰ to 0.4‰) was slightly higher than that of the OC seawater samples (−2.7‰ to −0.4‰) collected only during Legs 1–3. This difference was mainly due to the difference in the sampling periods, as the underway seawater dataset consisted of samples from Legs 4 and 5 with generally more depleted in $\delta^{18}O$. The largest isotopic range was found for lead water samples ($\delta^{18}O$ of −7.8‰ to 1.3‰; *d-excess* of −7.7‰ to 5.8‰).

Near-surface seawater samples collected daily from November 2019 to October 2020 for measuring the isotopic signature of the seawater along the *Polarstern* track were combined with continuous measurements of seawater salinity (Schmithüsen, 2021a). We found that, generally, the changes in seawater $\delta^{18}O$ were closely mimicked by changes in seawater salinity (**Figure 9b**).

At the beginning of the expedition in the Amundsen Basin at about 85°N, surface seawater had a $\delta^{18}O$ composition of around −1.5‰ and a salinity of 32.2. As the *Polarstern* drifted toward Fram Strait, seawater became increasingly depleted in $\delta^{18}O$ and less saline until mid-February (at 87°N, 91°W), when the lowest $\delta^{18}O$ value (−2.4‰) and salinity (31.7) were observed during Legs 1–3 (**Figure 9b**). After this minimum, $\delta^{18}O$ and salinity values increased to a maximum of −0.4‰ and 34.3, at the end of Leg 3 (May 16, 2020). The weekly sampled OC seawater $\delta^{18}O$ values show an almost identical pattern compared to the more highly resolved time series for underway seawater $\delta^{18}O$.

As *Polarstern* left the ice floe (Central Observatory) to Svalbard on May 17 for a 1-month break until June 17, $\delta^{18}O$ values during transit to Svalbard increased to an absolute maximum of 0.4‰, together with a maximum surface salinity of 33.9. At the start of Leg 4, *Polarstern* navigated back to the original ice floe and drifted south toward Fram Strait. During this time, $\delta^{18}O$ values became progressively lower, down to −2.2‰ at the end of Leg 4 (July 31; **Figure 9b**). Similarly, the seawater salinity during this period decreased to 31.3 (**Figure 9a**, **b**).

At the end of July, the ice floe broke apart in Fram Strait (79°N, 2.5°W) and *Polarstern* transited northward until it reached a location close to the North Pole (87°N, 104°E) in the Amundsen Basin, where the final part of the expedition, Leg 5, took place. Here, seawater $\delta^{18}O$ decreased from −1.1‰ to −3.0‰ during the first 10 days and after that ranged between −3.0‰ and −3.3‰ until the end of the campaign. Likewise, seawater salinity decreased from 32.1 to 29.2 in the first 10 days and then varied around 29. A more detailed study, focusing on ocean column properties such as temperature, salinity, and density, was conducted during MOSAiC by Schulz et al. (2023).

3.3.2. Water sources contributing to the surface waters during MOSAiC

The relationship between surface seawater $\delta^{18}O$ and mean daily salinity correlated significantly ($R^2 = 0.80$, p-value < 0.0001; **Figure 9**) throughout the entire MOSAiC period, with low $\delta^{18}O$ values associated with lower salinities. Except for Leg 2, the regression lines between $\delta^{18}O$ and salinity had similar slopes (0.7 to 0.9) but variable intercepts (−33‰ to −12‰; **Figure 9**). Throughout MOSAiC, seawater $\delta^{18}O$ values of −1.2‰ to −2.4‰ were observed consistently during all 5 legs, while the salinities varied between 30 and 34 (**Figure 9b**), contributing to different $\delta^{18}O$-salinity regressions. These seasonally and geographically changing relationships suggest that seawater isotopes were influenced by more than two sources in the Arctic Ocean, which had been investigated extensively (Östlund and Hut, 1984; Bauch et al., 1995; Ekwurzel et al., 2001; Yamamoto-Kawai et al., 2008; Bauch et al., 2011b; Newton et al., 2013).

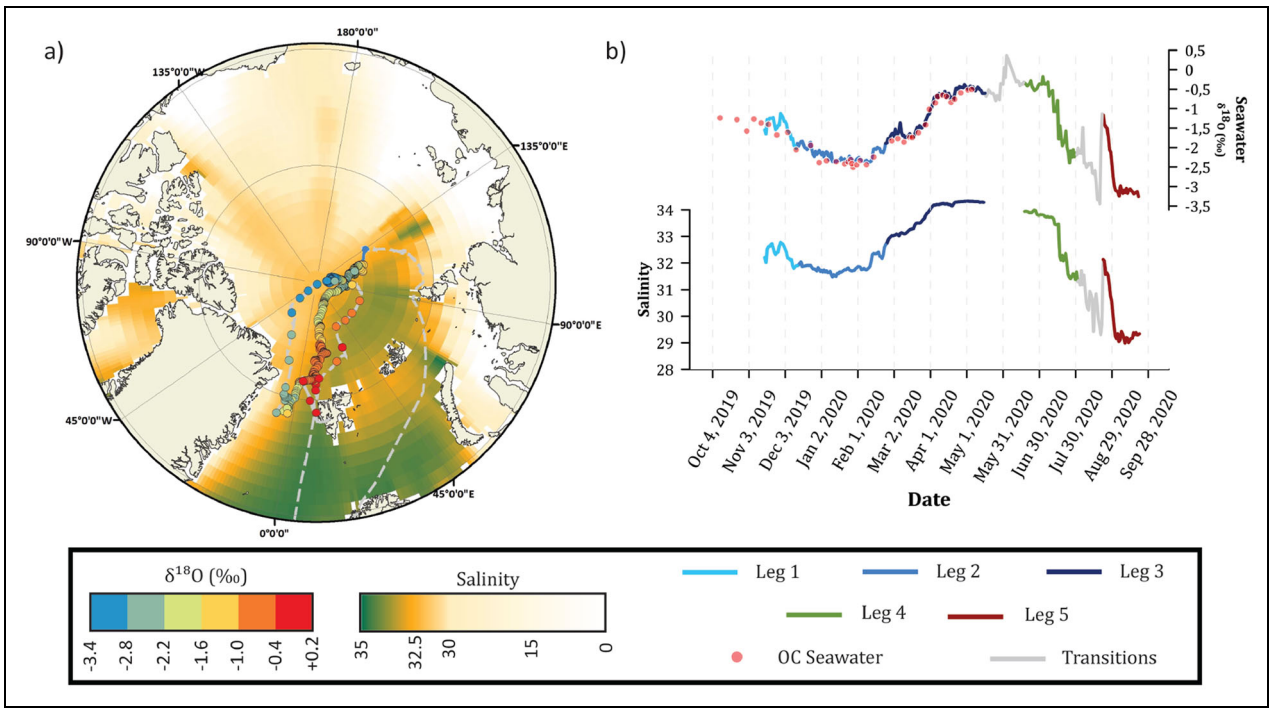

Figure 9. Underway seawater $\delta^{18}O$ and salinity during the MOSAiC expedition from October 2019 to September 2020. (a) Average seawater salinity in July 2020 from the World Ocean Atlas, NOAA (https://www.ncei.noaa.gov/access/world-ocean-atlas-2018), in color-coded shading, and $\delta^{18}O$ values for each individual underway seawater sample collected along the track of *Polarstern*, in color-coded dots. (b) Time series of seawater $\delta^{18}O$ (upper) and salinity (lower). The continuous measurements during Legs 1–3 are presented with different shades of blue, Leg 4 in green, and Leg 5 in brick red. The $\delta^{18}O$ and salinity of seawater measured during the transition periods between the legs are presented in grey. The red dots represent the surface seawater $\delta^{18}O$ measurements from site Ocean City collected weekly during Legs 1–3.

The Arctic Ocean receives water from various sources, including the Pacific and Atlantic Oceans, river inflow, glaciers, sea-ice meltwater, and local precipitation. Atlantic Water flows into the Arctic through Fram Strait, as well as through the Barents and Kara Seas (Aagaard and Carmack, 1989; Rudels et al., 2005). The inflow of relatively warm saline Atlantic water is associated with a relatively higher isotopic composition (Östlund and Hut, 1984; Legrande and Schmidt, 2006). We, therefore, assume a relatively strong influence of Atlantic waters in our data at the beginning of the expedition in the Amundsen Basin (85°N, 135°E), where seawater $\delta^{18}O$ was relatively high (about −1.5‰). The contribution of Atlantic Water to the Arctic Ocean was also noticeable during the transition period between Legs 3 and 4, when *Polarstern* left the ice floe and moved into the open waters to reach Svalbard (May 16 to June 17, $-0.8 < \delta^{18}O < 0.1$‰, 31.1 < salinity < 33.9). The other marine water source to the Arctic Ocean is Pacific inflow through the Bering Strait. However, because the MOSAiC expedition took place in the eastern sector of the Arctic Ocean, the potential effect of this water source may not be traceable in this study (Bauch et al., 2011b; Paffrath et al., 2021).

River discharge provides a freshwater source with a distinctively low isotopic composition (Yi et al., 2012). Siberian rivers (i.e., Lena, Yenisey, Ob) channel meteoric waters falling over the continent and release them into the Arctic Ocean through the Kara, Laptev, and East Siberian seas. The freshwater input from these rivers provides regionally low saline waters through the shelf seas to the Arctic Ocean. The depletion of seawater in $\delta^{18}O$ in the Arctic Ocean is known to be associated with river discharge (Solomon et al., 2021). In their seminal study, Cooper et al. (2008) conducted extensive observations of major Arctic Ocean inflowing rivers, revealing remarkably low isotopic compositions with $\delta^{18}O$ values as follows: −14.6‰, Ob; −17.5‰, Yenisey; −20‰, Lena; and −21.9‰, Kolyma. In October–November 2018, during the year preceding the MOSAiC expedition and, in a region, coinciding with the proximity of *Polarstern*, the $\delta^{18}O$ values of Lena River water were primarily within the range of −18‰ to −20‰ (Juhls et al., 2020). Freshwater was subsequently introduced into the Arctic Ocean, thereby contributing to the overall isotopic composition of the Arctic Ocean's water. When *Polarstern* drifted into the Nansen Basin, the surface seawater $\delta^{18}O$ and salinity rose to −0.4‰ and 34.3 (April 29), respectively. We attribute the isotopic enrichment to a gradual increase in the influence of Atlantic Water (and a decreasing influence of riverine meteoric water) during Leg 3.

The largest and most abrupt changes in seawater isotopic composition and salinity during the MOSAiC campaign occurred during Leg 4, when $\delta^{18}O$ and salinity decreased progressively (from around −0.3‰ to

−2.2‰; **Figure 9**) as *Polarstern* passed through Fram Strait on the edge of the sea ice into the East Greenland Current (EGC). The simultaneous decreasing change in salinity suggests the mixing of freshwater with ocean water in this region. The EGC flows along the continental slope of the Greenland Sea Shelf and transports freshwater and sea ice with low $\delta^{18}O$ from the Arctic Ocean toward the North Atlantic (Aagaard and Carmack, 1989; Rabe et al., 2014; Steur et al., 2018). In addition, the Greenland Ice Sheet releases meltwater and has been described as one of the freshwater sources contributing to low $\delta^{18}O$ (Dodd et al., 2012; Laukert et al., 2017) and salinity (Rudels et al., 2005). Greenland Ice Sheet meltwater is discharged into the North Atlantic at remarkable rates through the 79°N glacier, as documented by Huhn et al. (2021). The seawater collected in the vicinity of this release of glacier meltwater exhibited consistently low $\delta^{18}O$ values, with an average value of approximately −2.9‰ (±0.1, N = 7), and a low salinity mean of 31.3 (±0.4). Moreover, during Leg 4, the ice floe experienced an increase in melt ponds from sea ice and snow melt at the surface, accounting for up to 20% of the surface area by the end of July and accompanied by a drastic reduction in snow-covered areas (Webster et al., 2022). The continuous release of this fresh and isotopically light water throughout Leg 4 contributes to the gradual depletion of seawater in $\delta^{18}O$ while *Polarstern* was moving southward with the EGC. Due to similar $\delta^{18}O$ values of freshwater, contributions from river water, snow melt, or glacial melt cannot be distinguished (Dodd et al., 2012; Laukert et al., 2017).

The lowest salinity and $\delta^{18}O$ values during MOSAiC were recorded during Leg 5 (August and September 2020) close to the North Pole in the Amundsen Basin (87°N to 89°N). Compared to Atlantic Waters (Legrande and Schmidt, 2006), seawater in the sea-ice-covered area around the North Pole had a low (approximately −3‰) $\delta^{18}O$ composition. This low value points to a large contribution of freshwater to this region in the heart of the Arctic Ocean. Potential sources of light isotopic freshwater in the Arctic Ocean in Leg 5 were similar to those described before; that is, the Siberian riverine influx, local precipitation, and the snow on sea ice. However, slopes and intercepts between stable isotopes and salinity during Leg 5 are distinctly different from those of Legs 1–4 (**Figure 9**), suggesting at first glance the mixing of different endmembers. An endmember refers to a pure and distinct component within a mixture, representing an extreme or specific source with unique characteristics, often used in isotopic analysis to identify relative contributions from different sources or processes. But y-intercepts in the Arctic cannot be interpreted as endmembers due to the influence of sea-ice formation, which adds salt to the water column. The observed differences in correlations and slopes between datasets can be attributed to differences in geographical regions, as well as the seasonality of sea-ice melting and formation (Bauch et al., 2011a). However, the distinction between freshwater sources such as rivers and snow melt cannot be based solely on stable isotopic water signatures and cannot be further disentangled in this study.

3.4. Further studies of the hydrological components

In addition to snow, sea ice, and seawater, melt ponds, lead water, lead ice, and water vapor were sampled for isotopic measurements during the MOSAiC expedition. Each of these hydrological components provide additional and distinctive contributions to an understanding of the Arctic water cycle as a whole.

Melt ponds play a crucial role in the energy budget of Arctic sea ice, especially in spring and summer, as they absorb more solar radiation than the surrounding ice (Perovich et al., 1998). The isotopic composition of melt ponds in this study changed over time, due to the relative contributions of snow and sea ice melt, the evaporation from the pond surface, and refreezing. Generally, refrozen and open melt ponds had an intermediate isotopic signature compared to the surrounding sea ice and snow (**Table 1**), suggesting that they were a mixture of sea ice and snow melt. Similarities in the isotope composition of melt ponds and SYI suggest that this mixture in ponds could be involved as a first step in the formation of SYI (**Figure 10**). As outlined above, the isotopic composition of sea ice and snow changed over time due to the relative contributions of different water sources and due to the interaction between snow and sea ice, and these changes may be transferred into melt ponds as they became larger and deeper due to the continuous sea-ice melt (Zhang et al., 2018).

Lead water had slightly lower mean $\delta^{18}O$ (−2.3‰; **Table 1**) compared to lead ice (−1.2‰), seawater (−1.7‰), and FYI (−0.7‰), which could be a result of the contribution of freshwater at the surface during summer as suggested by Nomura et al. (2023). They studied lead effects on water structure during Leg 5 in the central Arctic, analyzing lead width, refreezing, and mixing. Melt ponds had similar $\delta^{18}O$ values to lead water samples and surrounding sea ice. The melting of sea ice resulted in the production of liquid water that displayed reduced $\delta^{18}O$ values compared to the remaining ice. This disparity arises from the selective liberation of lighter isotopes, specifically ^{16}O, in comparison to the heavier isotopes (^{18}O), which are released preferentially at a higher rate. Ice formation and melting change the salinity of seawater, influencing the $\delta^{18}O$ values of melt ponds. Melt pond formation causes dissolved oxygen concentration in seawater to decrease, changing the $\delta^{18}O$ values due to oxygen isotope exchange with the atmosphere. In our study, we observed that the mean *d-excess* of melt ponds (0.9‰) fell between the values for FYI (0.5‰) and SYI (1.6‰), with the rather low melt pond $\delta^{18}O$ values (mean = −2.1‰) suggesting the contribution of snow to melt ponds.

Brunello et al. (2023) investigated the continuous water vapor isotopic composition in the Arctic during MOSAiC, revealing seasonal variations in $\delta^{18}O$ and *d-excess*. The authors found that the changes in the isotopic composition of the summer moisture correlated with temperature and humidity over open ocean sectors, and that they were controlled largely by evaporative conditions over the source regions. In contrast,

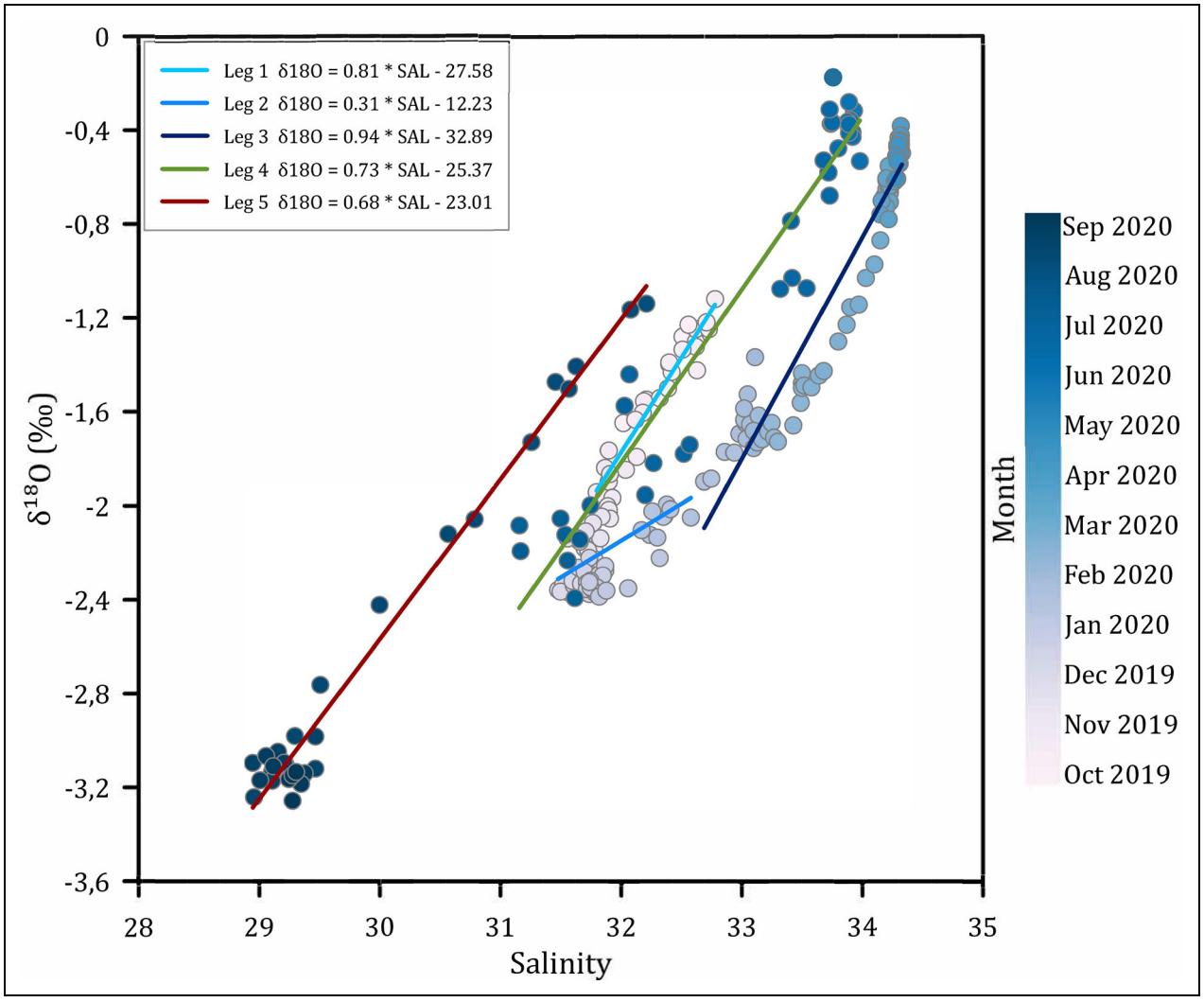

Figure 10. Surface seawater $\delta^{18}O$ versus salinity during the 5 legs of MOSAiC. The circles represent daily seawater measurements, color-coded based on the month (October 2019 to September 2020) during which the samples were collected. The calculated surface seawater $\delta^{18}O$-salinity regression for each leg is provided, with regression lines color-coded by leg.

winter moisture could not be explained solely by source conditions and appears to be influenced by moisture exchange processes during the transport and the long residence over the sea ice. Coupling these results with isotopic composition data from discrete samples of sea ice, seawater, snow, and melt ponds can lead to a better understanding of the regional impacts of Arctic water exchange processes.

4. Conclusions

Climate change causes profound alterations of the Arctic region. The isotopic composition of the hydrological components informs us on the dynamics and processes involved in the Arctic water cycle, contributing to an assessment of the current state and future changes in response to ongoing warming. In this study, we have presented the isotopic composition ($\delta^{18}O$, $\delta^{2}H$) of the different water components in the central Arctic Ocean, as observed during the MOSAiC drifting expedition in 2019–2020. The overall dataset includes 2200 samples and provides a statistical overview of the isotopic composition of sea ice, seawater, snow, melt ponds, and other parts of the Arctic hydrological cycle. Both spatial and temporal gradients were studied with a focus of surface seawater, sea ice, and snow on top of the sea ice.

We found that the $\delta^{18}O$ values of *snow* gradually increased from the surface to the bottom of the snowpack, whereas *d-excess* values decreased. This gradient is visible in most snow profiles, independently of time and location of sampling. The higher $\delta^{18}O$ and lower *d-excess* values in the middle and bottom layers of the snowpack indicate a smaller contribution from meteoric water with depth and a significant impact from the underlying sea ice surface. Even at the snow surface, where fresh precipitation would be added, air temperatures were not correlated with the surface snow $\delta^{18}O$ values. Thus, the contribution of meteoric waters (e.g., fresh snowfall) was either very limited or had been modified after deposition. Additionally, the continuous depletion of *d-excess* from October 2019 through July 2020 (e.g., **Figure 5a**) was associated

with the snow-sea ice interaction and the sublimation processes at this interface. These findings suggest the need for further investigation into the effects of snow metamorphic processes on the isotopic composition of snow on top of the sea ice.

The *surface seawater* isotopic composition and salinities across the Arctic Ocean during the MOSAiC expedition indicate different water sources that contributed with distinct isotopic signatures. Our analysis showed a strong correlation between salinity and $\delta^{18}O$. The geographical as well as seasonal shifts in salinity and $\delta^{18}O$ correlation suggest that seawater isotopes can be used to infer the relative contributions of distinct water masses to the whole Arctic Ocean. Significant contributions are Atlantic Ocean waters mixing with fresh water influxes from Siberian rivers (Legs 1, 2), and the melt of snow together with freshwater input from sea-ice melt and influx from the Greenland ice sheet (Legs 4, 5). These contributions lead to regionally and seasonally different, specific Arctic surface seawater isotopic compositions and salinities.

The isotopic composition of *sea ice* provides useful information about different formation mechanisms, and the key role of sea ice in the Arctic Ocean's water cycle. FYI was typically more enriched in $\delta^{18}O$ than SYI due to various factors, including freezing and post-freezing modifications. The sea-ice isotopic composition was influenced by factors such as lower surface seawater $\delta^{18}O$ values at the time of formation and evaporation from melt ponds, resulting in lower salinity and $\delta^{18}O$. In contrast, iFYI, which forms during the winter season at the bottom of SYI, generally had a higher isotopic composition than SYI due to similar factors that contribute to the heavier isotope composition of FYI compared to SYI. A threshold of approximately -2‰ separated the iFYI from the upper SYI layer. Our results show that the isotopic compositions help to distinguish between ocean-sourced FYI and iFYI from SYI with a meteoric contribution. Moreover, they offer crucial insights into the isotopic dynamics between snow and sea ice in the central Arctic.

In summary, seawater, sea ice, and snow as key components of the Arctic water cycle interact with each other as well as with more transient constituents such as melt ponds, leads, and frost flowers to provide insight into local exchange processes with the atmosphere. These findings deepen our understanding of the intricate interactions between atmosphere, sea ice, and ocean in this region and underscore the need for comprehensive and coordinated isotopic data collection across diverse Arctic locations and seasons. Such a collaborative approach is vital as we face complex challenges posed by climate change in the Arctic.

Data accessibility statement

All data in this manuscript are publicly available from online repositories. The data can be found under the following references:

- Stable water isotopes of underway seawater during the MOSAiC expedition (Mellat et al., 2022b).
- Stable water isotopes of snow during MOSAiC expedition (Mellat et al., 2022a).
- Stable water isotopes and conductivities of a lead case study during Leg 5 of the MOSAiC expedition (Meyer et al., 2022).
- Stable water isotopes of seawater at site Ocean City during MOSAiC expedition (Mellat et al., 2023a).
- Stable water isotopes of sea ice at multiple coring stations (MCS) during the MOSAiC expedition (Mellat et al., 2023b).
- Overview of physical oceanography measurements during *Polarstern* cruise PS122—MOSAiC (Tippenhauer et al., 2021).
- Continuous meteorological surface measurement during *Polarstern* cruise PS122/1-2-3-4-5 (Schmithüsen, 2021a, 2021b, 2021c, 2021d, 2021e).
- Master tracks in different resolutions of *Polarstern* cruise PS122/1-2-3-4-5 (Haas, 2020; Kanzow, 2020; Rex, 2020, 2021a, 2021b).

Supplemental files

The supplemental files for this article can be found as follows:

Figures S1 and S2. PDF

Acknowledgments

The authors would like to express their gratitude to the International Multidisciplinary Drifting Observatory for the Study of the Arctic Climate (MOSAiC) with the tag MOSAiC20192020 for providing the opportunity to conduct this research and for producing the data used in this report. Specifically, they would like to thank all people who were involved in this expedition of the Research Vessel *Polarstern* (Knust, 2017) and helped to collect the samples during MOSAiC in the 2019–2020 project (Project ID: AWI_PS122_00) (Nixdorf et al., 2021). They extend their sincere appreciation to all the persons involved in the expedition of the R/V *Polarstern* during MOSAiC in 2019–2020 (AWI_PS122_00). They also thank Mikaela Weiner and Andreas Marent for analyzing the isotopic compositions ($\delta^{18}O$, $\delta^{2}H$) of the samples in the ISOLAB Facility at AWI in Potsdam. They also extend their thanks to the two anonymous reviewers whose insightful and constructive feedback contributed to the improvement of the manuscript's structure and clarity. They also acknowledge support by the Open Access Publication Funds of Alfred-Wegener-Institut Helmholtz-Zentrum für Polar- und Meeresforschung.

Funding

MM, CFB, MW, and HM are grateful for the support provided by the German Federal Ministry of Education and Research (project MOSAiC-CiASOM, grant number 03F0869A). DB received support from the German science foundation (DFG grant BA1689/4). MAG received support from The Research Council of Norway (project HAVOC, grant no. 280292). DN received support from the Japan Society for the Promotion of Science (grant numbers: JP18H03745; JP18KK0292; JP17KK0083; JP17H04715; JP20H04345) and a grant from the Joint Research Program of the Japan Arctic Research Network

Center. SA was funded by the German Research Council (DFG) in the framework of the priority program "Antarctic Research with comparative investigations in Arctic Ice areas" (Grant Nos. SPP1158 and AR1236/1), the Emmy Noether Grant of the DFG (AR 1236/2-1/493362232) and by the Alfred-Wegener-Institut, Helmholtz-Zentrum fuür Polar-und Meeresforschung.

Competing interests

All authors declare that they have no competing interests.

Author contributions

Contributed to conception and design: MM, HM, CFB, MW, DB, MAG, JMW.

Contributed to acquisition of data: MM, HM, CFB, MW, DB, ED, MA, DN, JMW, MS, MAG, MH, ARM, SA.

Contributed to analysis and interpretation of data: MM, HM, CFB, MW, DB, MAG, MA, JMW.

Drafted and/or revised the article: MM, HM, MW, CFB, DB, MAG, ARM, DN, MA, JMW, MS, SA, MH, ED.

Approved the submitted version for publication: All Authors.

References

Aagaard, K, **Carmack, EC.** 1989. The role of sea ice and other fresh water in the Arctic circulation. *Journal of Geophysical Research* **94**(C10): 14485. DOI: http://dx.doi.org/10.1029/jc094ic10p14485.

Aemisegger, F, **Trachsel, J**, **Sadowski, Y**, **Eichler, A**, **Lehning, M**, **Avak, S**, **Schneebeli, M.** 2022. Fingerprints of frontal passages and post-depositional effects in the stable water isotope signal of seasonal Alpine snow. *Journal of Geophysical Research: Atmospheres* **127**(22). DOI: http://dx.doi.org/10.1029/2022jd037469.

Akers, PD, **Kopec, BG**, **Mattingly, KS**, **Klein, ES**, **Causey, D**, **Welker, JM.** 2020. Baffin Bay sea ice extent and synoptic moisture transport drive water vapor isotope ($\delta^{18}O$, $\delta^{2}H$, and deuterium excess) variability in coastal northwest Greenland. *Atmospheric Chemistry and Physics* **20**(22): 13929–13955. DOI: http://dx.doi.org/10.5194/acp-20-13929-2020.

Ala-aho, P, **Welker, JM**, **Bailey, H**, **Pedersen, SH**, **Kopec, B**, **Klein, E**, **Mellat, M**, **Mustonen, K-R**, **Noor, K**, **Marttila, H**. 2021. Arctic snow isotope hydrology: A comparative snow-water vapor study. *Atmosphere* **12**(2): 150. DOI: http://dx.doi.org/10.3390/atmos12020150.

Angelopoulos, M, **Damm, E**, **Simões Pereira, P**, **Abrahamsson, K**, **Bauch, D**, **Bowman, J**, **Castellani, G**, **Creamean, J**, **Divine, DV**, **Dumitrascu, A**, **Fons, SW**, **Granskog, MA**, **Kolabutin, N**, **Krumpen, T**, **Marsay, C**, **Nicolaus, M**, **Oggier, M**, **Rinke, A**, **Sachs, T**, **Shimanchuk, E**, **Stefels, J**, **Stephens, M**, **Ulfsbo, A**, **Verdugo, J**, **Wang, L**, **Zhan, L**, **Haas, C.** 2022. Deciphering the properties of different Arctic ice types during the growth phase of MOSAiC: Implications for future studies on gas pathways. *Frontiers in Earth Science* **10**: 864523. DOI: http://dx.doi.org/10.3389/feart.2022.864523.

Arctic Monitoring and Assessment Programme. 2017. *Snow, water, ice and permafrost in the Arctic (SWIPA) 2017*. Oslo, Norway: Arctic Monitoring and Assessment Programme (AMAP).

Aron, PG, **Li, S**, **Brooks, JR**, **Welker, JM**, **Levin, NE.** 2023. Seasonal variations in triple oxygen isotope ratios of precipitation in the western and central United States. *Paleoceanography and Paleoclimatology* **38**(4). DOI: http://dx.doi.org/10.1029/2022pa004458.

Bailey, H, **Hubbard, A**, **Klein, ES**, **Mustonen, K-R**, **Akers, PD**, **Marttila, H**, **Welker, JM.** 2021. Arctic sea-ice loss fuels extreme European snowfall. *Nature Geoscience* **14**(5): 283–288. DOI: http://dx.doi.org/10.1038/s41561-021-00719-y.

Bailey, HL, **Klein, ES**, **Welker, JM.** 2019. Synoptic and mesoscale mechanisms drive winter precipitation $\delta^{18}O/\delta^{2}H$ in south-central Alaska. *Journal of Geophysical Research: Atmospheres* **124**(7): 4252–4266. DOI: http://dx.doi.org/10.1029/2018jd030050.

Barber, DG, **Ehn, JK**, **Pućko, M**, **Rysgaard, S**, **Deming, JW**, **Bowman, JS**, **Papakyriakou, T**, **Galley, RJ**, **Søgaard, DH.** 2014. Frost flowers on young Arctic sea ice: The climatic, chemical, and microbial significance of an emerging ice type. *Journal of Geophysical Research: Atmospheres* **119**(20): 11593–11612. DOI: http://dx.doi.org/10.1002/2014jd021736.

Bauch, D, **Cherniavskaia, E**, **Timokhov, L.** 2016. Shelf basin exchange along the Siberian continental margin: Modification of Atlantic water and lower halocline water. *Deep Sea Research Part I: Oceanographic Research Papers* **115**: 188–198.

Bauch, D, **Dmitrenko, IA**, **Wegner, C**, **Hölemann, J**, **Kirillov, SA**, **Timokhov, LA**, **Kassens, H.** 2009. Exchange of Laptev Sea and Arctic Ocean halocline waters in response to atmospheric forcing. *Journal of Geophysical Research* **114**(C5). DOI: http://dx.doi.org/10.1029/2008jc005062.

Bauch, D, **Hölemann, J**, **Andersen, N**, **Dobrotina, E**, **Nikulina, A**, **Kassens, H.** 2011a. The Arctic shelf regions as a source of freshwater and brine-enriched waters as revealed from stable oxygen isotopes. *Polarforschung* **80**(3): 127–140.

Bauch, D, **Schlosser, P**, **Fairbanks, RG.** 1995. Freshwater balance and the sources of deep and bottom waters in the Arctic Ocean inferred from the distribution of $H_2{}^{18}O$. *Progress in Oceanography* **35**(1): 53–80. DOI: http://dx.doi.org/10.1016/0079-6611(95)00005-2.

Bauch, D, **van der Loeff, MR**, **Andersen, N**, **Torres-Valdes, S**, **Bakker, K**, **Abrahamsen, EP.** 2011b. Origin of freshwater and polynya water in the Arctic Ocean halocline in summer 2007. *Progress in Oceanography* **91**(4): 482–495. DOI: http://dx.doi.org/10.1016/j.pocean.2011.07.017.

Beck, N, **Münnich, KO.** 1988. Freezing of water: Isotopic fractionation. *Chemical Geology* **70**(1–2): 168.

Beria, H, **Larsen, JR**, **Ceperley, NC**, **Michelon, A**, **Vennemann, T**, **Schaefli, B.** 2018. Understanding snow hydrological processes through the lens of stable

water isotopes. *WIREs Water* **5**(6): e1311. DOI: http://dx.doi.org/10.1002/wat2.1311.

Bowen, GJ, **Cai, Z**, **Fiorella, RP**, **Putman, AL.** 2019. Isotopes in the water cycle: Regional- to global-scale patterns and applications. *Annual Review of Earth and Planetary Sciences* **47**(1): 453–479. DOI: http://dx.doi.org/10.1146/annurev-earth-053018-060220.

Brunello, CF, **Meyer, H**, **Mellat, M**, **Casado, M**, **Bucci, S**, **Dütsch, M**, **Werner, M.** 2023. Contrasting seasonal isotopic signatures of near-surface atmospheric water vapour in the Central Arctic during the MOSAiC campaign. *Journal of Geophysical Research: Atmospheres* **128**(24): e2022JD038400. DOI: http://dx.doi.org/10.1029/2022JD038400.

Casado, M, **Landais, A**, **Picard, G**, **Arnaud, L**, **Dreossi, G**, **Stenni, B**, **Prié, F.** 2021. Water isotopic signature of surface snow metamorphism in Antarctica. *Geophysical Research Letters* **48**(17): e2021GL093382. DOI: http://dx.doi.org/10.1029/2021gl093382.

Chemke, R, **Polvani, LM**, **Kay, JE**, **Orbe, C.** 2021. Quantifying the role of ocean coupling in Arctic amplification and sea-ice loss over the 21st century. *npj Climate and Atmospheric Science* **4**(1): 46. DOI: http://dx.doi.org/10.1038/s41612-021-00204-8.

Cooper, LW, **Benner, R**, **McClelland, JW**, **Peterson, BJ**, **Holmes, RM**, **Raymond, PA**, **Hansell, DA**, **Grebmeier, JM**, **Codispoti, LA.** 2005. Linkages among runoff, dissolved organic carbon, and the stable oxygen isotope composition of seawater and other water mass indicators in the Arctic Ocean. *Journal of Geophysical Research: Biogeosciences* **110**(G2). DOI: http://dx.doi.org/10.1029/2005jg000031.

Cooper, LW, **McClelland, JW**, **Holmes, RM**, **Raymond, PA**, **Gibson, JJ**, **Guay, CK**, **Peterson, BJ.** 2008. Flow-weighted values of runoff tracers ($\delta^{18}O$, DOC, Ba, alkalinity) from the six largest Arctic rivers. *Geophysical Research Letters* **35**(18). DOI: http://dx.doi.org/10.1029/2008gl035007.

Craig, H. 1961. Isotopic variations in meteoric waters. *Science* **133**(3465): 1702–1703. DOI: http://dx.doi.org/10.1126/science.133.3465.1702.

Csank, AZ, **Czimczik, CI**, **Xu, X**, **Welker, JM.** 2019. Seasonal patterns of riverine carbon sources and export in NW Greenland. *Journal of Geophysical Research: Biogeosciences* **124**(4): 840–856. DOI: http://dx.doi.org/10.1029/2018jg004895.

Dansgaard, W. 1964. Stable isotopes in precipitation. *Tellus* **16**(4): 436–468. DOI: http://dx.doi.org/10.3402/tellusa.v16i4.8993.

Deser, C, **Teng, H.** 2008. Evolution of Arctic sea ice concentration trends and the role of atmospheric circulation forcing, 1979–2007. *Geophysical Research Letters* **35**(2). DOI: http://dx.doi.org/10.1029/2007gl032023.

Dodd, PA, **Rabe, B**, **Hansen, E**, **Falck, E**, **Mackensen, A**, **Rohling, E**, **Stedmon, C**, **Kristiansen, S.** 2012. The freshwater composition of the Fram Strait outflow derived from a decade of tracer measurements. *Journal of Geophysical Research: Oceans* **117**(C11). DOI: http://dx.doi.org/10.1029/2012jc008011.

Douglas, TA, **Domine, F**, **Barret, M**, **Anastasio, C**, **Beine, HJ**, **Bottenheim, J**, **Grannas, A**, **Houdier, S**, **Netcheva, S**, **Rowland, G**, **Staebler, R**, **Steffen, A.** 2012. Frost flowers growing in the Arctic ocean-atmosphere–sea ice–snow interface: 1 Chemical composition. *Journal of Geophysical Research: Atmospheres* **117**(D14). DOI: http://dx.doi.org/10.1029/2011jd016460.

Dubinina, EO, **Kossova, SA**, **Miroshnikov, AY**, **Kokryatskaya, NM.** 2017. Isotope (δD, $\delta^{18}O$) systematics in waters of the Russian Arctic seas. *Geochemistry International* **55**(11): 1022–1032. DOI: http://dx.doi.org/10.1134/s0016702917110052.

Dutton, A, **Wilkinson, BH**, **Welker, JM**, **Bowen, GJ**, **Lohmann, KC.** 2005. Spatial distribution and seasonal variation in $^{18}O/^{16}O$ of modern precipitation and river water across the conterminous USA. *Hydrological Processes* **19**(20): 4121–4146. DOI: http://dx.doi.org/10.1002/hyp.5876.

Ebner, PP, **Steen-Larsen, HC**, **Stenni, B**, **Schneebeli, M**, **Steinfeld, A.** 2017. Experimental observation of transient $\delta^{18}O$ interaction between snow and advective airflow under various temperature gradient conditions. *The Cryosphere* **11**(4): 1733–1743. DOI: http://dx.doi.org/10.5194/tc-11-1733-2017.

Eicken, H. 1998. Deriving modes and rates of ice growth in the Weddell Sea from microstructural, salinity and stable-isotope data. *Antarctic Sea Ice: Physical Processes, Interactions and Variability, Antarctic Research Series* **74**: 89–122.

Ekwurzel, B, **Schlosser, P**, **Mortlock, RA**, **Fairbanks, RG**, **Swift, JH.** 2001. River runoff, sea ice meltwater, and Pacific water distribution and mean residence times in the Arctic Ocean. *Journal of Geophysical Research: Oceans* **106**(C5): 9075–9092. DOI: http://dx.doi.org/10.1029/1999jc000024.

Friedman, I, **Benson, C**, **Gleason, J**. 1991. Isotopic changes during snow metamorphism, in Taylor, HP, O'Neil, JR, Kaplan, IR eds., *Stable isotope geochemistry: A tribute to Samuel Epstein.* San Antonio, TX: The Geochemical Society: 211–222.

Galewsky, J, **Steen-Larsen, HC**, **Field, RD**, **Worden, J**, **Risi, C**, **Schneider, M.** 2016. Stable isotopes in atmospheric water vapor and applications to the hydrologic cycle. *Reviews of Geophysics* **54**(4): 809–865. DOI: http://dx.doi.org/10.1002/2015rg000512.

Gat, JR. 1996. Oxygen and hydrogen isotopes in the hydrologic cycle. *Annual Review of Earth and Planetary Sciences* **24**(1): 225–262. DOI: http://dx.doi.org/10.1146/annurev.earth.24.1.225.

Granskog, MA, **Rösel, A**, **Dodd, PA**, **Divine, D**, **Gerland, S**, **Martma, T**, **Leng, MJ.** 2017. Snow contribution to first-year and second-year Arctic sea ice mass balance north of Svalbard. *Journal of Geophysical Research: Oceans* **122**(3): 2539–2549. DOI: http://dx.doi.org/10.1002/2016jc012398.

Haas, C. 2020. Links to master tracks in different resolutions of POLARSTERN cruise PS122/2. Arctic

Ocean–Arctic Ocean, 2019-12-13–2020-02-24 (Version 2) [dataset]. DOI: http://dx.doi.org/10.1594/PANGAEA.924674.

Hanisco, TF, **Moyer, EJ**, **Weinstock, EM**, **St Clair, JM**, **Sayres, DS**, **Smith, JB**, **Lockwood, R**, **Anderson, JG**, **Dessler, AE**, **Keutsch, FN**, **Spackman, JR**, **Read, G**, **Bui, TP**. 2007. Observations of deep convective influence on stratospheric water vapor and its isotopic composition. *Geophysical Research Letters* **34**(4). DOI: http://dx.doi.org/10.1029/2006gl027899.

Hersbach, H, **Bell, B**, **Berrisford, P**, **Hirahara, S**, **Horányi, A**, **Muñoz-Sabater, J**, **Nicolas, J**, **Peubey, C**, **Radu, R**, **Schepers, D**, **Simmons, A**, **Soci, C**, **Abdalla, S**, **Abellan, X**, **Balsamo, G**, **Bechtold, P**, **Biavati, G**, **Bidlot, J**, **Bonavita, M**, **De Chiara, G**, **Dahlgren, P**, **Dee, D**, **Diamantakis, M**, **Dragani, R**, **Flemming, J**, **Forbes, R**, **Fuentes, M**, **Geer, A**, **Haimberger, L**, **Healy, S**, **Hogan, RJ**, **Hólm, E**, **Janisková, M**, **Keeley, S**, **Laloyaux, P**, **Lopez, P**, **Lupu, C**, **Radnoti, G**, **de Rosnay, P**, **Rozum, I**, **Vamborg, F**, **Villaume, S**, **Thépaut, J-N**. 2020. The ERA5 global reanalysis. *Quarterly Journal of the Royal Meteorological Society* **146**(730): 1999–2049. DOI: http://dx.doi.org/10.1002/qj.3803.

Hoffmann, G, **Jouzel, J**, **Masson, V.** 2000. Stable water isotopes in atmospheric general circulation models. *Hydrological Processes* **14**(8): 1385–1406.

Huhn, O, **Rhein, M**, **Kanzow, T**, **Schaffer, J**, **Sültenfuß, J.** 2021. Submarine meltwater from Nioghalvfjerdsbræ (79 North Glacier), Northeast Greenland. *Journal of Geophysical Research: Oceans* **126**(7): e2021JC017224. DOI: http://dx.doi.org/10.1029/2021jc017224.

Jafari, M, **Gouttevin, I**, **Couttet, M**, **Wever, N**, **Michel, A**, **Sharma, V**, **Rossmann, L**, **Maass, N**, **Nicolaus, M**, **Lehning, M.** 2020. The impact of diffusive water vapor transport on snow profiles in deep and shallow snow covers and on sea ice. *Frontiers in Earth Science* **8**: 249.

Johnsen, SJ, **Dansgaard, W**, **White, JWC.** 1989. The origin of Arctic precipitation under present and glacial conditions. *Tellus B: Chemical and Physical Meteorology* **41**(4): 452–468. DOI: http://dx.doi.org/10.3402/tellusb.v41i4.15100.

Jouzel, J. 2003. Water stable isotopes: Atmospheric composition and applications in polar ice core studies. *Treatise on Geochemistry* **4**: 347.

Jouzel, J, **Petit, J-R**, **Souchez, R**, **Barkov, N**, **Lipenkov, VY**, **Raynaud, D**, **Stievenard, M**, **Vassiliev, NI**, **Verbeke, V**, **Vimeux, F.** 1999. More than 200 meters of lake ice above subglacial Lake Vostok, Antarctica. *Science* **286**(5447): 2138–2141.

Juhls, B, **Stedmon, CA**, **Morgenstern, A**, **Meyer, H**, **Hölemann, J**, **Heim, B**, **Povazhnyi, V**, **Overduin, PP.** 2020. Identifying drivers of seasonality in Lena River biogeochemistry and dissolved organic matter fluxes. *Frontiers in Environmental Science* **8**: 53. DOI: http://dx.doi.org/10.3389/fenvs.2020.00053.

Kanzow, T. 2020. Links to master tracks in different resolutions of Polarstern cruise PS122/3. Arctic Ocean–Longyearbyen, 2020-02-24–2020-06-04 (Version 2) [dataset]. DOI: http://doi.org/10.1594/PANGAEA.924681.

Klein, ES, **Cherry, JE**, **Young, J**, **Noone, D**, **Leffler, AJ**, **Welker, JM.** 2015. Arctic cyclone water vapor isotopes support past sea ice retreat recorded in Greenland ice. *Scientific Reports* **5**(1): 10295. DOI: http://dx.doi.org/10.1038/srep10295.

Klein, ES, **Welker, JM.** 2016. Influence of sea ice on ocean water vapor isotopes and Greenland ice core records. *Geophysical Research Letters* **43**(24): 12475–12483. DOI: http://dx.doi.org/10.1002/2016gl071748.

Knust, R. 2017. Polar research and supply vessel POLARSTERN operated by the Alfred-Wegener-Institute. *Journal of Large-Scale Research Facilities JLSRF* **3**: A119. DOI: http://dx.doi.org/10.17815/jlsrf-3-163.

Krumpen, T, **Birrien, F**, **Kauker, F**, **Rackow, T**, **Von Albedyll, L**, **Angelopoulos, M**, **Belter, HJ**, **Bessonov, V**, **Damm, E**, **Dethloff, K**, **Haapala, J**, **Haas, C**, **Harris, C**, **Hendricks, S**, **Hoelemann, J**, **Hoppmann, M**, **Kaleschke, L**, **Karcher, M**, **Kolabutin, N**, **Lei, R**, **Lenz, J**, **Morgenstern, A**, **Nicolaus, M**, **Nixdorf, U**, **Petrovsky, T**, **Rabe, B**, **Rabenstein, L**, **Rex, M**, **Ricker, R**, **Rohde, J**, **Shimanchuk, E**, **Singha, S**, **Smolyanitsky, V**, **Sokolov, V**, **Stanton, T**, **Timofeeva, A**, **Tsamados, M**, **Watkins, D.** 2020. The MOSAiC ice floe: Sediment-laden survivor from the Siberian shelf. *The Cryosphere* **14**(7): 2173–2187. DOI: http://dx.doi.org/10.5194/tc-14-2173-2020.

Krumpen, T, **Von Albedyll, L**, **Goessling, HF**, **Hendricks, S**, **Juhls, B**, **Spreen, G**, **Willmes, S**, **Belter, HJ**, **Dethloff, K**, **Haas, C**, **Kaleschke, L**, **Katlein, C**, **Tian-Kunze, X**, **Ricker, R**, **Rostosky, P**, **Rückert, J**, **Singha, S**, **Sokolova, J**. 2021. MOSAiC drift expedition from October 2019 to July 2020: Sea ice conditions from space and comparison with previous years. *The Cryosphere* **15**(8): 3897–3920. DOI: http://dx.doi.org/10.5194/tc-15-3897-2021.

Lange, BA, **Haas, C**, **Mucci, A**, **Beckers, JF**, **Casey, JA**, **Duerksen, S**, **Granskog, MA**, **Hatam, I**, **Niemi, A**, **Reppchen, A**, **Michel, C.** 2021. Contribution of snow to Arctic first-year and multi-year sea ice mass balance within the Last Ice Area. *Journal of Geophysical Research: Oceans* **126**(5): e2020JC016971. DOI: http://dx.doi.org/10.1029/2020jc016971.

Laukert, G, **Frank, M**, **Bauch, D**, **Hathorne, EC**, **Rabe, B**, **von Appen, WJ**, **Wegner, C**, **Zieringer, M**, **Kassens, H.** 2017. Ocean circulation and freshwater pathways in the Arctic Mediterranean based on a combined Nd isotope, REE and oxygen isotope section across Fram Strait. *Geochimica et Cosmochimica Acta* **202**: 285–309. DOI: http://dx.doi.org/10.1016/j.gca.2016.12.028.

Legrande, AN, **Schmidt, GA.** 2006. Global gridded data set of the oxygen isotopic composition in seawater. *Geophysical Research Letters* **33**(12). DOI: http://dx.doi.org/10.1029/2006gl026011.

Lehmann, M, **Siegenthaler, U.** 1991. Equilibrium oxygen- and hydrogen-isotope fractionation between ice and water. *Journal of Glaciology* **37**(125): 23–26. DOI: http://dx.doi.org/10.3189/s0022143000042751.

Lindsay, R, **Schweiger, A.** 2015. Arctic sea ice thickness loss determined using subsurface, aircraft, and satellite observations. *The Cryosphere* **9**(1): 269–283. DOI: http://dx.doi.org/10.5194/tc-9-269-2015.

Mellat, M, **Bailey, H**, **Mustonen, K-R**, **Marttila, H**, **Klein, ES**, **Gribanov, K**, **Bret-Harte, MS**, **Chupakov, AV**, **Divine, DV**, **Else, B**, **Filippov, I**, **Hyöky, V**, **Jones, S**, **Kirpotin, SN**, **Kroon, A**, **Markussen, HT**, **Nielsen, M**, **Olsen, M**, **Paavola, R**, **Pokrovsky, OS**, **Prokushkin, A**, **Rasch, M**, **Raundrup, K**, **Suominen, O**, **Syvänperä, I**, **Vignisson, SR**, **Zarov, E**, **Welker, JM**. 2021. Hydroclimatic controls on the isotopic ($\delta^{18}O$, $\delta^{2}H$, d-excess) traits of pan-Arctic summer rainfall events. *Frontiers in Earth Science* **9**(367): 651731. DOI: http://dx.doi.org/10.3389/feart.2021.651731.

Mellat, M, **Meyer, H**, **Bauch, D**, **Damm, E**, **Werner, M**, **Brunello, CF**, **Weiner, M**, **Marent, A.** 2023a. Stable water isotopes of seawater at Ocean City during MOSAiC expedition [dataset]. PANGAEA. DOI: http://dx.doi.org/10.1594/PANGAEA.958464.

Mellat, M, **Meyer, H**, **Brunello, CF**, **Arndt, S**, **Macfarlane, AR**, **Schneebeli, M**, **Hörhold, M**, **Werner, M**, **Weiner, M**, **Marent, A.** 2022a. Stable water isotopes of snow during MOSAiC expedition [dataset]. Bremerhaven, Germany: Alfred Wegener Institute for Polar and Marine Research. PANGAEA. DOI: http://dx.doi.org/10.1594/PANGAEA.948511.

Mellat, M, **Meyer, H**, **Brunello, CF**, **Werner, M**, **Dahlke, S**, **Sommerfeld, A**, **Deckelmann, H**, **Jaiser, R**, **Weiner, M**, **Marent, A.** 2022b. Stable water isotopes of underway seawater during MOSAiC expedition [dataset]. Bremerhaven, Germany: Alfred Wegener Institute for Polar and Marine Research. PANGAEA. DOI: http://dx.doi.org/10.1594/PANGAEA.948291.

Mellat, M, **Meyer, H**, **Werner, M**, **Brunello, CF**, **Granskog, MA**, **Damm, E**, **Bauch, D**, **Weiner, M**, **Marent, A.** 2023b. Stable water isotopes of sea ice at Multiple Coring Stations (MCS) during MOSAiC expedition [dataset]. PANGAEA. DOI: http://dx.doi.org/10.1594/PANGAEA.958466.

Meyer, H, **Mellat, M**, **Nomura, D**, **Damm, E**, **Bauch, D**, **Weiner, M**, **Marent, A.** 2022. Stable water isotopes and conductivities of a lead case study during leg 5 of the MOSAiC expedition [dataset]. PANGAEA. DOI: http://dx.doi.org/10.1594/PANGAEA.945285.

Meyer, H, **Schönicke, L**, **Wand, U**, **Hubberten, HW**, **Friedrichsen, H.** 2000. Isotope studies of hydrogen and oxygen in ground ice—Experiences with the equilibration technique. *Isotopes in Environmental and Health Studies* **36**(2): 133–149. DOI: http://dx.doi.org/10.1080/10256010008032939.

Newton, R, **Schlosser, P**, **Mortlock, R**, **Swift, J**, **Macdonald, R.** 2013. Canadian basin freshwater sources and changes: Results from the 2005 Arctic Ocean section. *Journal of Geophysical Research: Oceans* **118**(4): 2133–2154. DOI: http://dx.doi.org/10.1002/jgrc.20101.

Nicolaus, M, **Perovich, DK**, **Spreen, G**, **Granskog, MA**, **Von Albedyll, L**, **Angelopoulos, M**, **Anhaus, P**, **Arndt, S**, **Belter, JH**, **Bessonov, V**, **Birnbaum, G**, **Brauchle, J**, **Calmer, R**, **Cardellach, E**, **Cheng, B**, **Clemens-Sewall, B**, **Dadic, R**, **Damm, E**, **de Boer, G**, **Demir, O**, **Dethloff, K**, **Divine, DV**, **Fong, AA**, **Fons, S**, **Frey, MM**, **Fuchs, N**, **Gabarró, C**, **Gerland, S**, **Goessling, HF**, **Gradinger, R**, **Haapala, J**, **Haas, C**, **Hamilton, J**, **Hannula, H-R**, **Hendricks, S**, **Herber, A**, **Heuzé, C**, **Hoppmann, M**, **Høyland, KV**, **Huntemann, M**, **Hutchings, JK**, **Hwang, B**, **Itkin, P**, **Jacobi, H-W**, **Jaggi, M**, **Jutila, A**, **Kaleschke, L**, **Katlein, C**, **Kolabutin, N**, **Krampe, D**, **Savstrup Kristensen, S**, **Krumpen, T**, **Kurtz, N**, **Lampert, A**, **Lange, BA**, **Lei, B**, **Light, B**, **Linhardt, F**, **Liston, GE**, **Loose, B**, **Macfarlane, AR**, **Mahmud, M**, **Matero, IO**, **Maus, S**, **Morgenstern, A**, **Naderpour, R**, **Nandan, V**, **Niubom, A**, **Oggier, M**, **Oppelt, N**, **Pätzold, F**, **Perron, C**, **Petrovsky, T**, **Pirazzini, R**, **Polashenski, C**, **Rabe, B**, **Raphael, IA**, **Regnery, J**, **Rex, M**, **Ricker, R**, **Riemann-Campe, K**, **Rinke, A**, **Rohde, J**, **Salganik, E**, **Scharien, RK**, **Schiller, M**, **Schneebeli, M**, **Semmling, M**, **Shimanchuk, E**, **Shupe, MD**, **Smith, MM**, **Smolyanitsky, V**, **Sokolov, V**, **Stanton, T**, **Stroeve, J**, **Thielke, L**, **Timofeeva, A**, **Tage Tonboe, R**, **Tavri, A**, **Tsamados, M**, **Wagner, DN**, **Watkins, D**, **Webster, M**, **Wendisch M**. 2022. Overview of the MOSAiC expedition: Snow and sea ice. *Elementa: Science of the Anthropocene* **10**(1). DOI: http://dx.doi.org/10.1525/elementa.2021.000046.

Nixdorf, U, **Dethloff, K**, **Rex, M**, **Shupe, M**, **Sommerfeld, A**, **Perovich, DK**, **Nicolaus, M**, **Heuzé, C**, **Rabe, B**, **Loose, B**, **Damm, E**, **Gradinger, R**, **Fong, A**, **Maslowski, W**, **Rinke, A**, **Kwok, R**, **Spreen, G**, **Wendisch, M**, **Herber, A**, **Hirsekorn, M**, **Mohaupt, V**, **Frickenhaus, S**, **Immerz, A**, **Weiss-Tuider, K**, **König, B**, **Mengedoht, D**, **Regnery, J**, **Gerchow, P**, **Ransby, D**, **Krumpen, T**, **Morgenstern, A**, **Haas, C**, **Kanzow, T**, **Rack, FR**, **Saitzev, V**, **Sokolov, V**, **Makarov, A**, **Schwarze, S**, **Wunderlich, T**, **Wurr, K**, **Boetius, A**. 2021. MOSAiC extended acknowledgement. DOI: http://dx.doi.org/10.5281/zenodo.5541624.

Nomura, D, **Kawaguchi, Y**, **Webb, AL**, **Li, Y**, **Dall'osto, M**, **Schmidt, K**, **Doroste, ES**, **Chamberlain, EJ**, **Kolabuting, N**, **Shimanchuk, E**, **Hoppmann, M**, **Gallagher, MR**, **Meyer, H**, **Mellat, M**, **Bauch, D**, **Gabarró, C**, **Smith, MM**, **Inoue, J**, **Damm, E**, **Delille, B.** 2023. Meltwater layer dynamics in a central Arctic lead: Effects of lead width, re-freezing, and mixing during late summer. *Elementa: Science of the Anthropocene* **11**(1).

Notz, D, **Worster, MG.** 2008. In situ measurements of the evolution of young sea ice. *Journal of Geophysical Research* **113**(C3). DOI: http://dx.doi.org/10.1029/2007jc004333.

Östlund, HG, **Hut, G.** 1984. Arctic Ocean water mass balance from isotope data. *Journal of Geophysical Research* **89**(C4): 6373. DOI: http://dx.doi.org/10.1029/jc089ic04p06373.

Overland, J, **Hanna, E**, **Hanssen-Bauer, I**, **Kim, S**, **Walsh, J**, **Wang, M**, **Bhatt, US**, **Thoman, RL**, **Ballinger, TJ**. 2019. Surface air temperature Arctic report card 5. *NOAA*.

Paffrath, R, **Laukert, G**, **Bauch, D**, **Rutgers van der Loeff, M**, **Pahnke, K**. 2021. Separating individual contributions of major Siberian rivers in the transpolar drift of the Arctic Ocean. *Scientific Reports* **11**(1): 1–11.

Parkinson, CL, **DiGirolamo, NE.** 2021. Sea ice extents continue to set new records: Arctic, Antarctic, and global results. *Remote Sensing of Environment* **267**: 112753.

Perovich, DK, **Richter-Menge, JA.** 1994. Surface characteristics of lead ice. *Journal of Geophysical Research* **99**(C8): 16341. DOI: http://dx.doi.org/10.1029/94jc01194.

Perovich, DK, **Roesler, CS**, **Pegau, WS.** 1998. Variability in Arctic sea ice optical properties. *Journal of Geophysical Research: Oceans* **103**(C1): 1193–1208. DOI: http://dx.doi.org/10.1029/97jc01614.

Pfahl, S, **Sodemann, H.** 2014. What controls deuterium excess in global precipitation? *Climate of the Past* **10**(2): 771–781. DOI: http://dx.doi.org/10.5194/cp-10-771-2014.

Pinzer, B, **Schneebeli, M**, **Kaempfer, T.** 2012. Vapor flux and recrystallization during dry snow metamorphism under a steady temperature gradient as observed by time-lapse micro-tomography. *The Cryosphere Discussions* **6**(3): 1673–1714.

Polyakov, IV, **Pnyushkov, AV**, **Carmack, EC**. 2018. Stability of the arctic halocline: A new indicator of arctic climate change. *Environmental Research Letters* **13**(12): 125008.

Pörtner, H-O, **Roberts, DC**, **Parmesan, C**, **Adams, H**, **Adelekan, I**, **Adler, C**, **Adrian, R**, **Aldunce, P**, **Ali, E**, **Ara, R**, **Bednar-Friedl, B**. 2022. Climate change 2022: Impacts, adaptation and vulnerability. *IPCC Sixth Assessment Report*. Available at https://www.ipcc.ch/report/ar6/wg2/. Accessed November 16, 2022.

Puntsag, T, **Mitchell, MJ**, **Campbell, JL**, **Klein, ES**, **Likens, GE**, **Welker, JM.** 2016. Arctic Vortex changes alter the sources and isotopic values of precipitation in northeastern US. *Scientific Reports* **6**(1): 22647. DOI: http://dx.doi.org/10.1038/srep22647.

Rabe, B, **Heuzé, C**, **Regnery, J**, **Aksenov, Y**, **Allerholt, J**, **Athanase, M**, **Bai, Y**, **Basque, C**, **Bauch, D**, **Baumann, TM**, **Chen, D**, **Cole, ST**, **Craw, L**, **Davies, A**, **Damm, E**, **Dethloff, K**, **Divine, DV**, **Doglioni, F**, **Ebert, F**, **Fang, Y-C**, **Fer, I**, **Fong, AA**, **Gradinger, R**, **Granskog, MA**, **Graupner, R**, **Haas, C**, **He, H**, **He, Y**, **Hoppmann, M**, **Janout, M**, **Kadko, D**, **Kanzow, T**, **Karam, S**, **Kawaguchi, Y**, **Koenig, Z**, **Kong, B**, **Krishfield, RA**, **Krumpen, T**, **Kuhlmey, D**, **Kuznetsov, I**, **Lan, M**, **Laukert, G**, **Lei, R**, **Li, T**, **Torres-Valdés, S**, **Lin, L**, **Lin, L**, **Liu, H**, **Liu, N**, **Loose, B**, **Ma, X**, **MacKay, R**, **Mallet, M**, **Mallett, RDC**, **Maslowski, W**, **Mertens, C**, **Mohrholz, V**, **Muilwijk, M**, **Nicolaus, M**, **O'Brien, JK**, **Perovich, D**, **Ren, J**, **Rex, M**, **Ribeiro, N**, **Rinke, A**, **Schaffer, J**, **Schuffenhauer, I**, **Schulz, K**, **Shupe, MD**, **Shaw, W**, **Sokolov, V**, **Sommerfeld, A**, **Spreen, G**, **Stanton, T**, **Stephens, M**, **Su, J**, **Sukhikh, N**, **Sundfjord, A**, **Thomisch, K**, **Tippenhauer, S**, **Toole, JM**, **Vredenborg, M**, **Walter, M**, **Wang, H**, **Wang, L**, **Wang, Y**, **Wendisch, M**, **Zhao, J**, **Zhou, M**, **Zhu, J**. 2022. Overview of the MOSAiC expedition: Physical oceanography. *Elementa: Science of the Anthropocene* **10**(1). DOI: http://dx.doi.org/10.1525/elementa.2021.00062.

Rabe, B, **Karcher, M**, **Kauker, F**, **Schauer, U**, **Toole, JM**, **Krishfield, RA**, **Pisarev, S**, **Kikuchi, T**, **Su, J.** 2014. Arctic Ocean basin liquid freshwater storage trend 1992–2012. *Geophysical Research Letters* **41**(3): 961–968. DOI: http://dx.doi.org/10.1002/2013gl058121.

Rex, M. 2020. Links to master tracks in different resolutions of POLARSTERN cruise PS122/1. Tromsø–Arctic Ocean, 2019-09-20–2019-12-13 (Version 2) [dataset]. DOI: http://dx.doi.org/10.1594/PANGAEA.924668.

Rex, M. 2021a. Master tracks in different resolutions of POLARSTERN cruise PS122/4. Longyearbyen–Arctic Ocean, 2020-06-04–2020-08-12 [dataset]. DOI: http://dx.doi.org/10.1594/PANGAEA.926829.

Rex, M. 2021b. Master tracks in different resolutions of POLARSTERN cruise PS122/5. Arctic Ocean–Bremerhaven, 2020-08-12–2020-10-12 [dataset]. DOI: http://dx.doi.org/10.1594/PANGAEA.926910.

Rieke, O, **Årthun, M**, **Dörr, JS.** 2023. Rapid sea ice changes in the future Barents Sea. *The Cryosphere* **17**(4): 1445–1456. DOI: http://dx.doi.org/10.5194/tc-17-1445-2023.

Rozanski, K, **Araguas-Araguas, L**, **Gonfiantini, R.** 1992. Relation between long-term trends of oxygen-18 isotope composition of precipitation and climate. *Science* **258**(5084): 981–985. DOI: http://dx.doi.org/10.1126/science.258.5084.981.

Rudels, B, **Björk, G**, **Nilsson, J**, **Winsor, P**, **Lake, I**, **Nohr, C.** 2005. The interaction between waters from the Arctic Ocean and the Nordic Seas north of Fram Strait and along the East Greenland current: Results from the Arctic Ocean-02 Oden expedition. *Journal of Marine Systems* **55**(1–2): 1–30.

Salganik, E, **Lange, BA**, **Itkin, P**, **Divine, D**, **Katlein, C**, **Nicolaus, M**, **Hoppmann, M**, **Neckel, N**, **Ricker, R**, **Høyland, KV**, **Granskog, MA.** 2023. Different mechanisms of Arctic first-year sea-ice ridge consolidation observed during the MOSAiC expedition. *Elementa: Science of the Anthropocene* **11**(1). DOI: http://dx.doi.org/10.1525/elementa.2023.00008.

Schmithüsen, H. 2021a. Continuous meteorological surface measurement during Polarstern cruise PS122/1 [dataset]. PANGAEA. DOI: http://dx.doi.org/10.1594/PANGAEA.935221.

Schmithüsen, H. 2021b. Continuous meteorological surface measurement during Polarstern cruise PS122/2 [dataset]. Bremerhaven, Germany: Alfred Wegener Institute. PANGAEA. DOI: http://dx.doi.org/10.1594/PANGAEA.935222.

Schmithüsen, H. 2021c. Continuous meteorological surface measurement during Polarstern cruise PS122/3 [dataset]. Bremerhaven, Germany: Alfred Wegener Institute. PANGAEA. DOI: http://dx.doi.org/10.1594/PANGAEA.935223.

Schmithüsen, H. 2021d. Continuous meteorological surface measurement during Polarstern cruise PS122/4 [dataset]. Bremerhaven, Germany: Alfred Wegener Institute. PANGAEA. DOI: http://dx.doi.org/10.1594/PANGAEA.935224.

Schmithüsen, H. 2021e. Continuous meteorological surface measurement during Polarstern cruise PS122/5 [dataset]. Bremerhaven, Germany: Alfred Wegener Institute. PANGAEA. DOI: http://dx.doi.org/10.1594/PANGAEA.935225.

Schulz, K, **Koenig, Z**, **Muilwijk, M**, **Bauch, D**, **Hoppe, CJ**, **Droste, E**, **Hoppmann, M**, **Chamberlain, EJ**, **Laukert, G**, **Stanton, T**, **Zurita, AQ**, **Fer, I**, **Heuzé, C**, **Karam, S**, **Mieruch-Schnuelle, S**, **Baumann, T**, **Vredenborg, M**, **Tippenhauer, S**, **Granskog, MA**. 2023. The Eurasian Arctic Ocean along the MOSAiC drift (2019–2020): An interdisciplinary perspective on properties and processes. *Eartharxiv.org.* preprint.

Screen, JA, **Deser, C**, **Smith, DM**, **Zhang, X**, **Blackport, R**, **Kushner, PJ**, **Oudar, T**, **McCusker, KE**, **Sun, L.** 2018. Consistency and discrepancy in the atmospheric response to Arctic sea-ice loss across climate models. *Nature Geoscience* **11**(3): 155–163. DOI: http://dx.doi.org/10.1038/s41561-018-0059-y.

Serreze, MC, **Barrett, AP**, **Slater, AG**, **Woodgate, RA**, **Aagaard, K**, **Lammers, RB**, **Steele, M**, **Moritz, R**, **Meredith, M**, **Lee, CM.** 2006. The large-scale freshwater cycle of the Arctic. *Journal of Geophysical Research* **111**(C11). DOI: http://dx.doi.org/10.1029/2005jc003424.

Shupe, MD, **Rex, M**, **Blomquist, B**, **Persson, POG**, **Schmale, J**, **Uttal, T**, **Althausen, D**, **Angot, H**, **Archer, S**, **Bariteau, L**, **Beck, I**, **Bilberry, J**, **Bucci, S**, **Buck, C**, **Boyer, M**, **Brasseur, Z**, **Brooks, IM**, **Calmer, R**, **Cassano, J**, **Castro, V**, **Chu, D**, **Costa, D**, **Cox, CJ**, **Creamean, J**, **Crewell, S**, **Dahlke, S**, **Damm, E**, **de Boer, G**, **Deckelmann, H**, **Dethloff, K**, **Dütsch, M**, **Ebell, K**, **Ehrlich, A**, **Ellis, J**, **Engelmann, R**, **Fong, AA**, **Frey, MM**, **Gallagher, MR**, **Ganzeveld, L**, **Gradinger, R**, **Graeser, J**, **Greenamyer, V**, **Griesche, H**, **Griffiths, S**, **Hamilton, J**, **Heinemann, G**, **Helmig, D**, **Herber, A**, **Heuzé, C**, **Hofer, J**, **Houchens, T**, **Howard, D**, **Inoue, J**, **Jacobi, H-W**, **Jaiser, R**, **Jokinen, T**, **Jourdan, O**, **Jozef, G**, **King, W**, **Kirchgaessner, A**, **Klingebiel, M**, **Krassovski, M**, **Krumpen, T**, **Lampert, A**, **Landing, W**, **Laurila, T**, **Lawrence, D**, **Lonardi, M**, **Loose, B**, **Lüpkes, C**, **Maahn, M**, **Macke, A**, **Maslowski, W**, **Marsay, C**, **Maturilli, M**, **Mech, M**, **Morris, S**, **Moser, M**, **Nicolaus, M**, **Ortega, P**, **Osborn, J**, **Pätzold, F**, **Perovich, DK**, **Petäjä, T**, **Pilz, C**, **Pirazzini, R**, **Posman, K**, **Powers, H**, **Pratt, KA**, **Preußer, A**, **Quéléver, L**, **Radenz, M**, **Rabe, B**, **Rinke, A**, **Sachs, T**, **Schulz, A**, **Siebert, H**, **Silva, T**, **Solomon, A**, **Sommerfeld, A**, **Spreen, G**, **Stephens, M**, **Stohl, A**, **Svensson, G**, **Uin, J**, **Viegas, J**, **Voigt, C**, **von der Gathen, P**, **Wehner, B**, **Welker, JM**, **Wendisch, M**, **Werner, M**, **Xie, ZQ**, **Yue, F**. 2022. Overview of the MOSAiC expedition: Atmosphere. *Elementa: Science of the Anthropocene* **10**(1): 00060. DOI: http://dx.doi.org/10.1525/elementa.2021.00060.

Smith, MM, **von Albedyll, L**, **Raphael, IA**, **Lange, BA**, **Matero, I**, **Salganik, E**, **Webster, MA**, **Granskog, MA**, **Fong, A**, **Lei, R**, **Light, B.** 2022. Quantifying false bottoms and under-ice meltwater layers beneath Arctic summer sea ice with fine-scale observations. *Elementa: Science of the Anthropocene* **10**(1): 000116. DOI: http://dx.doi.org/10.1525/elementa.2021.000116.

Solomon, A, **Heuzé, C**, **Rabe, B**, **Bacon, S**, **Bertino, L**, **Heimbach, P**, **Inoue, J**, **Iovino, D**, **Mottram, R**, **Zhang, X**, **Aksenov, Y**, **McAdam, R**, **Nguyen, A**, **Raj, RP**, **Tang H.** 2021. Freshwater in the Arctic Ocean 2010–2019. *Ocean Science* **17**(4): 1081–1102. DOI: http://dx.doi.org/10.5194/os-17-1081-2021.

Sommerfeld, RA, **Judy, C**, **Friedman, I.** 1991. Isotopic changes during the formation of depth hoar in experimental snowpacks. *Stable Isotope Geochemistry* **3**: 205–209.

Steen-Larsen, HC, **Masson-Delmotte, V**, **Hirabayashi, M**, **Winkler, R**, **Satow, K**, **Prié, F**, **Bayou, N**, **Brun, E**, **Cuffey, KM**, **Dahl-Jensen, D**, **Dumont, M**, **Guillevic, M**, **Kipfstuhl, S**, **Landais, A**, **Popp, T**, **Risi, C**, **Steffen, K**, **Stenni, B**, **Sveinbjörnsdottír, AE.** 2014. What controls the isotopic composition of Greenland surface snow? *Climate of the Past* **10**(1): 377–392. DOI: http://dx.doi.org/10.5194/cp-10-377-2014.

Steur, L, **Peralta-Ferriz, C**, **Pavlova, O**. 2018. Freshwater export in the East Greenland current freshens the North Atlantic. *Geophysical Research Letters* **45**(24). DOI: http://dx.doi.org/10.1029/2018gl080207.

Stichler, W, **Rauert, W**, **Martinec, J.** 1981. Environmental isotope studies of an alpine snowpack. *Hydrology Research* **12**(4–5): 297–308.

Stroeve, JC, **Kattsov, V**, **Barrett, A**, **Serreze, M**, **Pavlova, T**, **Holland, M**, **Meier, WN.** 2012. Trends in Arctic sea ice extent from CMIP5, CMIP3 and observations. *Geophysical Research Letters* **39**(16). DOI: http://dx.doi.org/10.1029/2012gl052676.

Sturm, M, **Benson, CS.** 1997. Vapor transport, grain growth and depth-hoar development in the subarctic snow. *Journal of Glaciology* **43**(143): 42–59. DOI: http://dx.doi.org/10.3189/s0022143000002793.

Style, RW, **Worster, MG.** 2009. Frost flower formation on sea ice and lake ice. *Geophysical Research Letters* **36**(11). DOI: http://dx.doi.org/10.1029/2009gl037304.

Sun, J, **Liu, S**, **Cohen, J**, **Yu, S.** 2022. Influence and prediction value of Arctic sea ice for spring Eurasian extreme heat events. *Communications Earth & Environment* **3**(1). DOI: http://dx.doi.org/10.1038/s43247-022-00503-9.

Terzer-Wassmuth, S, **Wassenaar, LI**, **Welker, JM**, **Araguás-Araguás, LJ**. 2021. Improved high-resolution global and regionalized isoscapes of $\delta^{18}O$, $\delta^{2}H$ and *d*-excess in precipitation. *Hydrological Processes* **35**(6). DOI: http://dx.doi.org/10.1002/hyp.14254.

Tian, L, **Gao, Y**, **Ackley, SF**, **Stammerjohn, S**, **Maksym, T**, **Weissling, B.** 2018. Stable isotope clues to the formation and evolution of refrozen melt ponds on Arctic Sea ice. *Journal of Geophysical Research: Oceans* **123**(12): 8887–8901. DOI: http://dx.doi.org/10.1029/2018jc013797.

Tippenhauer, S, **Karam, S**, **Heuzé, C**, **Rabe, B.** 2021. Overview of physical oceanography measurements during Polarstern cruise PS122—MOSAiC [dataset]. PANGAEA. DOI: http://dx.doi.org/10.1594/PANGAEA.936275.

Toyota, T, **Smith, IJ**, **Gough, AJ**, **Langhorne, PJ**, **Leonard, GH**, **Van Hale, RJ**, **Mahoney, AR**, **Haskell, TG.** 2013. Oxygen isotope fractionation during the freezing of sea water. *Journal of Glaciology* **59**(216): 697–710.

Vihma, T, **Screen, J**, **Tjernström, M**, **Newton, B**, **Zhang, X**, **Popova, V**, **Deser, C**, **Holland, M**, **Prowse, T.** 2016. The atmospheric role in the Arctic water cycle: A review on processes, past and future changes, and their impacts. *Journal of Geophysical Research: Biogeosciences* **121**(3): 586–620. DOI: http://dx.doi.org/10.1002/2015jg003132.

Wahl, S, **Steen-Larsen, HC**, **Hughes, AG**, **Dietrich, LJ**, **Zuhr, A**, **Behrens, M**, **Faber, A-K**, **Hörhold, M**. 2022. Atmosphere-snow exchange explains surface snow isotope variability. *Geophysical Research Letters* **49**(20): e2022GL099529. DOI: http://dx.doi.org/10.1029/2022gl099529.

Wahl, S, **Steen-Larsen, HC**, **Reuder, J**, **Hörhold, M**. 2021. Quantifying the stable water isotopologue exchange between the snow surface and lower atmosphere by direct flux measurements. *Journal of Geophysical Research: Atmospheres* **126**(13). DOI: http://dx.doi.org/10.1029/2020jd034400.

Wang, Q, **Danilov, S**, **Jung, T**, **Kaleschke, L**, **Wernecke, A.** 2016. Sea ice leads in the Arctic Ocean: Model assessment, interannual variability and trends. *Geophysical Research Letters* **43**(13): 7019–7027. DOI: http://dx.doi.org/10.1002/2016gl068696.

Webster, MA, **Holland, M**, **Wright, NC**, **Hendricks, S**, **Hutter, N**, **Itkin, P**, **Light, B**, **Linhardt, F**, **Perovich, DK**, **Raphael, IA**, **Smith, MM**, **von Albedyll, L**, **Zhang, J.** 2022. Spatiotemporal evolution of melt ponds on Arctic sea ice: MOSAiC observations and model results. *Elementa: Science of the Anthropocene* **10**(1). DOI: http://dx.doi.org/10.1525/elementa.2021.000072.

Webster, MA, **Rigor, IG**, **Perovich, DK**, **Richter-Menge, JA**, **Polashenski, CM**, **Light, B**. 2015. Seasonal evolution of melt ponds on Arctic sea ice. *Journal of Geophysical Research: Oceans* **120**(9): 5968–5982. DOI: http://dx.doi.org/10.1002/2015jc011030.

Wefing, AM, **Casacuberta, N**, **Christl, M**, **Dodd, PA.** 2022. Water mass composition in Fram Strait determined from the combination of ^{129}I and ^{236}U: Changes between 2016, 2018, and 2019. *Frontiers in Marine Science* **9**. DOI: http://dx.doi.org/10.3389/fmars.2022.973507.

Welker, J. 2000. Isotopic ($\delta^{18}O$) characteristics of weekly precipitation collected across the USA: An initial analysis with application to water source studies. *Hydrological Processes* **14**(8): 1449–1464.

Welker, JM. 2012. ENSO effects on $\delta^{18}O$, $\delta^{2}H$ and *d-excess* values in precipitation across the U.S. using a high-density, long-term network (USNIP). *Rapid Communications in Mass Spectrometry* **26**(17): 1893–1898. DOI: http://dx.doi.org/10.1002/rcm.6298.

Winnick, MJ, **Chamberlain, CP**, **Caves, JK**, **Welker, JM.** 2014. Quantifying the isotopic 'continental effect'. *Earth and Planetary Science Letters* **406**: 123–133. DOI: http://dx.doi.org/10.1016/j.epsl.2014.09.005.

World Meteorological Organization. 2014. World Meteorological Organization (WMO) Sea Ice Nomenclature: WMO-No. 259 supplement to Vol. I, II and III, 5th Session of JCOMM Expert Team on Sea Ice. Technical Report. Geneva, Switzerland: World Meteorological Organization.

Yamamoto-Kawai, M, **McLaughlin, FA**, **Carmack, EC**, **Nishino, S**, **Shimada, K.** 2008. Freshwater budget of the Canada Basin, Arctic Ocean, from salinity, $\delta^{18}O$, and nutrients. *Journal of Geophysical Research* **113**(C1). DOI: http://dx.doi.org/10.1029/2006jc003858.

Yi, Y, **Gibson, JJ**, **Cooper, LW**, **Hélie, JF**, **Birks, SJ**, **McClelland, JW**, **Holmes, RM**, **Peterson, BJ.** 2012. Isotopic signals (^{18}O, ^{2}H, ^{3}H) of six major rivers draining the pan-Arctic watershed. *Global Biogeochemical Cycles* **26**(1). DOI: http://dx.doi.org/10.1029/2011gb004159.

Zhang, J, **Schweiger, A**, **Webster, M**, **Light, B**, **Steele, M**, **Ashjian, C**, **Campbell, R**, **Spitz, Y.** 2018. Melt pond conditions on declining Arctic sea ice over 1979–2016: Model development, validation, and results. *Journal of Geophysical Research: Oceans* **123**(11): 7983–8003.

Zuhr, AM, **Wahl, S**, **Steen-Larsen, HC**, **Hörhold, M**, **Meyer, H**, **Laepple, T**. 2023. A snapshot on the buildup of the stable water isotopic signal in the upper snowpack at EastGRIP on the Greenland Ice Sheet. *Journal of Geophysical Research: Earth Surface* **128**(2): e2022JF006767. DOI: http://dx.doi.org/10.1029/2022jf006767.

How to cite this article: Mellat, M, Brunello, CF, Werner, M, Bauch, D, Damm, E, Angelopoulos, M, Nomura, D, Welker, JM, Schneebeli, M, Granskog, MA, Hoerhold, M, Macfarlane, AR, Arndt, S, Meyer, H. 2024. Isotopic signatures of snow, sea ice, and surface seawater in the central Arctic Ocean during the MOSAiC expedition. *Elementa: Science of the Anthropocene* 12(1). DOI: https://doi.org/10.1525/elementa.2023.00078

Domain Editor-in-Chief: Jody W. Deming, University of Washington, Seattle, WA, USA

Guest Editor: Gunnar Spreen, Institute of Environmental Physics, University of Bremen, Bremen, Germany

Knowledge Domain: Ocean Science

Part of an Elementa Special Feature: The Multidisciplinary Drifting Observatory for the Study of Arctic Climate (MOSAiC)

Published: February 22, 2024 **Accepted:** December 22, 2023 **Submitted:** May 26, 2023

ELEMENTA Science of the Anthropocene

Elem Sci Anth is a peer-reviewed open access journal published by University of California Press.

OPEN ACCESS